Fluid flow in a spiral microfluidic duct

Brendan Harding[a] and Yvonne Stokes[b]
School of Mathematical Sciences, The University of Adelaide, Adelaide, SA 5005, Australia

(Received 19 February 2018; accepted 10 April 2018; published online 30 April 2018)

We consider the steady, pressure driven flow of a viscous fluid through a microfluidic device having the geometry of a planar spiral duct with a slowly varying curvature and height smaller than width. For this problem, it is convenient to express the Navier–Stokes equations in terms of a non-orthogonal coordinate system. Then, after applying appropriate scalings, the leading order equations admit a relatively simple solution in the central region of the duct cross section. First-order corrections with respect to the duct curvature and aspect ratio parameters are also obtained for this region. Additional correction terms are needed to ensure that no slip and no penetration conditions are satisfied on the side walls. Our solutions allow for a top wall shape that varies with respect to the radial coordinate which allows us to study the flow in a variety of cross-sectional shapes, including trapezoidal-shaped ducts that have been studied experimentally. At leading order, the flow is found to depend on the local height and slope of the top wall within the central region. The solutions are compared with numerical approximations of a classical Dean flow and are found to be in good agreement for a small duct aspect ratio and a slowly varying and small curvature. We conclude that the slowly varying curvature typical of spiral microfluidic devices has a negligible impact on the flow in the sense that locally the flow does not differ significantly from the classical Dean flow through a duct having the same curvature. *Published by AIP Publishing.* https://doi.org/10.1063/1.5026334

I. INTRODUCTION

Our interest in the fluid flow through a spiral duct is motivated by a desire to better understand particle focusing in microfluidic sorters. In general, microfluidic sorters are ducts of some appropriate shape, having micro-scale cross-sectional dimensions, through which a particle-laden fluid is forced; some examples may be found in the work of Martel and Toner.[1] Here we focus on the planar spiral ducts.

Segre and Silberberg[2] first observed the tendency of macroscopic spherical particles suspended in a laminar flow through a straight cylindrical tube to migrate toward an annulus with radius approximately 0.6 times the radius of the cylinder. Subsequent investigations spanning many decades attribute this tendency to opposing inertial lift forces acting on the particles which lead to equilibrium positions.[3–13] Di Carlo[14] refers to the opposing lift forces as a wall effect and shear-gradient-induced lift. Microfluidic sorters exploit these forces to focus and/or separate particles/cells suspended in a fluid. There is a considerable quantity of the experimental literature on microfluidic sorters having different designs; see the review of Martel and Toner.[1] Cross sections of microfluidic sorters (normal to the primary direction of flow) are typically rectangular in shape, although Warkiani *et al.*[15] considered a trapezoidal shape. Variations in duct geometry are, typically, combinations of varying the width and/or curvature of the duct, presumably because these are relatively straightforward to change. Analytical studies of inertial lift have largely been restricted to simple shear or parabolic flows and are difficult to extend to the complex three-dimensional flows that occur in a typical microfluidic sorter. Calculating a large number of particle trajectories via direct numerical simulation (DNS) with enough resolution to accurately determine the inertial lift forces is also infeasible for the long and complex channel geometries that are typical.[16] As such, numerical studies typically decouple the effect of the inertial lift and secondary flow to simplify computations.[17]

An alternative approach is to apply Lagrangian particle tracking to a flow field which is solved in the absence of particles. Several equations have been developed for approximating the motion of a particle based upon the flow field in the absence of particles, many of which are based on the models of Maxey and Riley[18] and Auton, Hunt, and Prud'Homme.[19] Whilst these and similar equations are reasonably accurate for simple shear and parabolic flows, they are much less accurate for more complex flows and finite-sized particles; see, for example, the results of Loth and Dorgan.[20] Additionally, such equations generally do not model the inertial lift effects which lead to particle focusing. An exception is the work of Liu *et al.*[16] which proposes an equation for the particle motion which includes a composite model of inertial lift forces. Combining such a model with a simple and accurate approximation of the particle free flow could facilitate a better understanding of how the geometry of the sorter influences the focusing and lead to improved designs.

In this paper, we study the pressure-driven Newtonian viscous flow in microfluidic ducts having a planar spiral geometry, in the absence of particles. Additionally, it will be assumed that a cross section of the duct (normal to the main direction of flow) has a small aspect ratio (defined to be height over half-width in this paper). The reason for this assumption is that

[a]brendan.harding@adelaide.edu.au
[b]yvonne.stokes@adelaide.edu.au

low aspect ratio ducts are common in the experimental literature; see, for example, the experiments of Martel and Toner[21] involving ducts of low to moderate aspect ratios. Additionally, low aspect ratio channels are known to be favourable for particle focusing in straight ducts where particles will migrate toward equilibrium positions which are a finite distance from the centre of the two longer walls.[22]

The viscous flow in curved pipes (with circular cross section) is a heavily studied topic in fluid dynamics going back to the early work of Dean.[23] The review article by Berger, Talbot, and Yao[23] covers many aspects known by the early 1980s. It is well understood that the curvature of the pipe gives rise to a secondary flow in the cross section of the pipe which has the effect of reducing the total rate of flow.[25] Helically wound pipes, having constant curvature and torsion, have also been studied.[26–31] Non-uniform curvature and torsion have also been studied in the context of blood flow.[32,33]

The viscous flow through pipes with non-circular cross sections has been studied to a lesser extent. A numerical bifurcation study was carried out by Winters[34] for curved rectangular ducts which found many different branching behaviours, albeit under Reynolds numbers much larger than those seen in typical microfluidic experiments and with height greater than or equal to width. Inspired by the coiled cochlea, Manoussaki and Chadwick[35] considered a steady inviscid flow in a helical duct with varying radius and square cross section.

Our interest in the flow through ducts with rectangular cross section is closely related to the work of Pozrikidis[36] and Norouzi and Biglari.[37] In the former, numerical solutions for the Stokes flow through circular and square ducts having a helical geometry were obtained using the finite element method on equations obtained via an asymptotic expansion in the cases of small and large pitch. On the other hand, Norouzi and Biglari[37] considered a rectangular duct with constant small curvature and zero torsion and obtained an analytical solution for several terms in a perturbation expansion with respect to a small curvature parameter via an application of Fourier methods.

The studies by Stokes *et al.*,[38] Lee, Stokes, and Bertozzi,[39] and Arnold, Stokes, and Green[40,41] of the thin-film viscous flow in open helically wound channels of rectangular and arbitrary cross-sectional shape with constant curvature and torsion, motivated by spiral particle separators used in mineral processing, are of particular relevance to the present work. Both helically wound channels and planar spiral ducts are used to segregate and focus particles of different size or density. However, the two problems differ in several key ways. Aside from the very different physical sizes of the devices, the planar spiral duct has zero torsion with the flow being driven by pressure and not gravity. Furthermore, there is no free surface and the duct has a changing curvature which we here assume to vary slowly with the arc length. We note that Manoussaki and Chadwick[35] effectively considered slowly varying curvature in their study of the cochlea, but their work assumed an inviscid fluid and, unlike the present work, ducts of rectangular cross-sectional shape only. We, however, assume cross sections of a small aspect ratio which they did not.

The flow in a spiral geometry is somewhat more difficult to solve than for geometries having constant curvature (including helical geometries) as one can no longer assume that the steady flow is invariant with respect to the angular coordinate (i.e., helically symmetric). However, we find that a slowly varying curvature does not significantly impact the leading order solution for the flow nor its first-order correction. In particular, the flow in any given cross section is close to that obtained if the curvature had been constant in a neighbourhood of the cross section. We also consider the effect on the flow if the top wall of the duct is not constant with respect to the radial coordinate. At leading order and away from the side walls, the flow in an infinitesimally thin vertical column of the cross section depends only on the height and slope of the duct at the top of that column. First-order corrections additionally depend on higher derivatives of the curve describing the top wall of the duct.

The paper is organised as follows. Section II develops the mathematical model from the Navier–Stokes equations expressed in a planar spiral coordinate system. The equations are then scaled and non-dimensionalised based upon the consideration of ducts having a large spiral radius relative to the half-width and a low aspect ratio. In Sec. III, we derive solutions to the leading order equations obtained from the scaling of the mathematical model. In Sec. IV, first-order corrections to the flow with respect to both the small curvature and aspect ratio are obtained. The derived solutions fail to satisfy the boundary conditions at the side walls, so this is remedied in Sec. V where it is illustrated how to obtain corrections in these regions. In Sec. VI, we plot and discuss the solutions for a variety of duct cross-sectional shapes. The effect of the different parameters on each velocity component is investigated and the solutions to the scaled model are compared to numerical solutions of the Dean flow[25] in Sec. VII. It is shown that the two are in good agreement for a variety of duct shapes over a range of curvature and aspect ratios.

II. MATHEMATICAL MODEL FOR FLOW IN A SPIRAL DUCT

Consider a steady, pressure-driven flow in a planar spiral duct, ignoring inlet and outlet regions. The governing equations of the fluid flow, with velocity $\mathbf{u}$, pressure p, density ρ, and viscosity μ, are the steady incompressible Navier–Stokes equations consisting of the momentum conservation equation

$$\rho\,(\mathbf{u}\cdot\nabla\mathbf{u}) = -\nabla p + \mu\nabla\cdot\left(\nabla\mathbf{u} + (\nabla\mathbf{u})^{\top}\right) \tag{1}$$

and the mass conservation (continuity) equation

$$\nabla\cdot\mathbf{u} = 0. \tag{2}$$

No slip boundary conditions ($\mathbf{u} = 0$) are enforced on all walls of the duct. We choose to use a coordinate system that permits a simple description of the flow geometry, as described below. Similar coordinate systems have been used by Manoussaki and Chadwick,[35] Stokes *et al.*,[38] Norouzi and Biglari,[37] Lee, Stokes, and Bertozzi,[39] and Arnold, Stokes, and Green[40] for rectangular ducts/channels with the bottom aligned horizontally in the radial direction.

A point in the fluid is defined by its radius R (measured horizontally from the centre of the spiral), angle β about the vertical axis through the spiral centre (taken here to be the

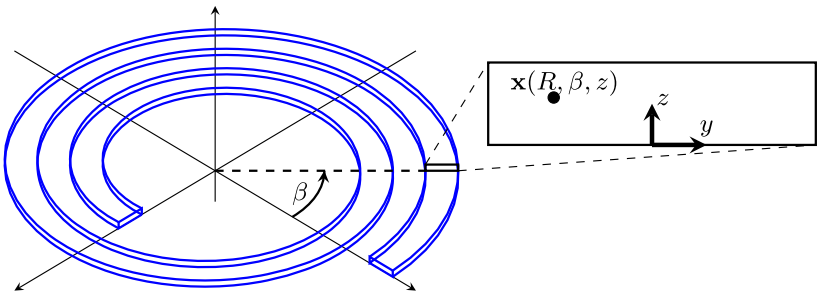

FIG. 1. Spiral duct with point **x** in fluid described by (R, β, z), where $R = A - \alpha\beta + y$.

origin), and vertical distance z from the plane $z = 0$; see Fig. 1. Specifically,

$$\mathbf{x}(R, \beta, z) = R\cos(\beta)\hat{\mathbf{i}} + R\sin(\beta)\hat{\mathbf{j}} + z\hat{\mathbf{k}}, \tag{3}$$

where $A_i(\beta) \le R \le A_o(\beta)$, with $A_i(\beta)$ and $A_o(\beta)$ being the location of the inner and outer vertical walls of the duct, respectively, and $h_b \le z \le h_t$, with h_b and h_t being the vertical positions of the bottom and top walls of the duct, respectively. We consider $A_i = (A - a) - \alpha\beta$, $A_o = (A + a) - \alpha\beta$ so that the duct is of constant width $2a$ with "centre-line" $(R, z) = (A - \alpha\beta, 0)$. The constant α denotes the rate at which the spiral radius changes with respect to the angle β. Our interest is tightly wound spirals in which α is small; although to ensure that the duct is not self-intersecting after one full turn, it is necessary that $|\alpha| > a/\pi$. In this paper, we focus on the case of increasing curvature with respect to β, i.e., positive α, although the results are analogous for the case of decreasing curvature. Given a positive α and supposing the spiral duct has $N > 0$ full rotations about the axis, then in order for the duct to avoid containing the origin (which would lead to self-intersection) we additionally require that

$$A - 2\pi N\alpha - a > 0 \quad \text{or} \quad \alpha < \frac{A - a}{2\pi N}. \tag{4}$$

For convenience, we parameterize R as $R = A - \alpha\beta + y$ from which it follows that, in any cross section (by which we mean a fixed angular position β), the radial variable y has the range $[-a, a]$. It is assumed that the cross section of the duct is the same at every β, that is, h_b, h_t are independent of β but may depend on y. We make the additional assumption $h_b = 0$ so that the bottom of the duct is flat and fixed at $z = 0$, while the top $h_t \equiv h(y)$ is allowed to vary with respect to y. In this setting, the centre-line along the bottom of the duct is the curve characterised by $(y, z) = (0, 0)$, that is, $\mathbf{x}(A - \alpha\beta, \beta, 0)$. To further put this into context, the microfluidic device used in the study of Warkiani *et al.*[15] is described by $a = 3/10$ mm, $A = 24$ mm, $\alpha = 1/\pi$ mm/rad, $h(y) = (63 + 50y)/600$ mm, and $N = 8$.

Given this general description of the spiral, the vector **x** may be re-parameterized as

$$\mathbf{x}(y, \beta, z) = (A - \alpha\beta + y)\cos(\beta)\hat{\mathbf{i}} + (A - \alpha\beta + y)\sin(\beta)\hat{\mathbf{j}} + z\hat{\mathbf{k}}. \tag{5}$$

Using this coordinate system, we obtain the continuity and steady incompressible Navier–Stokes equations using the general equations of Hill and Stokes[42] which are a reduced form of similar equations found in the work of Aris[43] and Wang.[26] In particular, with v, u, w denoting the flow velocities along the $\partial\mathbf{x}/\partial y$, $\partial\mathbf{x}/\partial\beta$, $\partial\mathbf{x}/\partial z$ vectors and $S = \sqrt{\alpha^2 + R^2}$, the resulting continuity equation is

$$\frac{\partial v}{\partial y} + \frac{\partial u}{\partial \beta} + \frac{\partial w}{\partial z} - \frac{\alpha}{R}u + \frac{1}{R}v = 0, \tag{6a}$$

and the momentum equations are

$$\rho\left[v\frac{\partial v}{\partial y} + u\frac{\partial v}{\partial \beta} + w\frac{\partial v}{\partial z} + \frac{2\alpha}{R}u(v - \alpha u) - Ru^2\right] = -\frac{S^2}{R^2}\frac{\partial p}{\partial y} - \frac{\alpha}{R^2}\frac{\partial p}{\partial \beta} + \mu\left\{\frac{S^2}{R^2}\frac{\partial^2 v}{\partial y^2} + \frac{1}{R^2}\left[\frac{\partial^2 v}{\partial \beta^2} + \left(\frac{2\alpha^2}{R} + R\right)\frac{\partial v}{\partial y} + \frac{2\alpha}{R}\frac{\partial v}{\partial \beta} - \frac{2\alpha^2 + 2R^2}{R}\frac{\partial u}{\partial \beta} - v + \alpha u\right] + \frac{\partial^2 v}{\partial z^2} + \frac{2\alpha}{R^2}\left[\frac{\partial^2 v}{\partial y \partial \beta} - \frac{\alpha^2}{R}\frac{\partial u}{\partial y}\right]\right\}, \tag{6b}$$

$$\rho\left[v\frac{\partial u}{\partial y} + u\frac{\partial u}{\partial \beta} + w\frac{\partial u}{\partial z} + \frac{2}{R}u(v - \alpha u)\right] = -\frac{\alpha}{R^2}\frac{\partial p}{\partial y} - \frac{1}{R^2}\frac{\partial p}{\partial \beta} + \mu\left\{\frac{S^2}{R^2}\frac{\partial^2 u}{\partial y^2} + \frac{1}{R^2}\left[\frac{\partial^2 u}{\partial \beta^2} + 3R\frac{\partial u}{\partial y} - \frac{2\alpha}{R}\frac{\partial u}{\partial \beta} + \frac{2}{R}\frac{\partial v}{\partial \beta}\right] + \frac{\partial^2 u}{\partial z^2} + \frac{2\alpha}{R^2}\left[\frac{\partial^2 u}{\partial y \partial \beta} + \frac{1}{R}\frac{\partial v}{\partial y} - \frac{\alpha}{R}\frac{\partial u}{\partial y}\right]\right\}, \tag{6c}$$

$$\rho\left[v\frac{\partial w}{\partial y} + u\frac{\partial w}{\partial \beta} + w\frac{\partial w}{\partial z}\right] = -\frac{\partial p}{\partial z} + \mu\left\{\frac{S^2}{R^2}\frac{\partial^2 w}{\partial y^2} + \frac{1}{R^2}\left[\frac{\partial^2 w}{\partial \beta^2} + R\frac{\partial w}{\partial y}\right] + \frac{\partial^2 w}{\partial z^2} + \frac{2\alpha}{R^2}\frac{\partial^2 w}{\partial y \partial \beta}\right\}. \tag{6d}$$

Furthermore, the physical velocity components are given by

$$(v, Su, w). \tag{7}$$

There are two scale parameters that are important in this problem. The duct height $h(y)$ is assumed to be small relative to the duct half-width a, and as such, we define the scaling parameter $\delta = H/a$, where the characteristic height H is taken to be the height at the centre of the duct, i.e., $H = h(0)$. Additionally, the duct half-width a is typically much smaller than the starting radius of the spiral A, and thus, the scaling parameter

$\epsilon = a/A$, sometimes referred to as the dimensionless curvature ratio (originating from studies of flow through curved cylindrical pipes), is defined. Utilising these two scaling parameters, we non-dimensionalise the governing equations via

$$(\beta, y, z) = (\beta, A\epsilon\hat{y}, A\epsilon\delta\hat{z}), \tag{8a}$$

$$(Su, v, w) = (U\hat{u}, U\epsilon\hat{v}, U\epsilon\delta\hat{w}), \tag{8b}$$

where dimensionless variables are denoted by carets and the characteristic velocity U is defined as the maximal physical axial velocity (i.e., Su) in the vertical column of fluid at $\beta = y = 0$. As the rate at which the spiral radius decreases needs only to be proportional to the duct width, we set $\alpha = A\epsilon\hat{\alpha}$. Similarly we non-dimensionalise $(R, S, h, H) = (A\hat{R}, A\hat{S}, A\epsilon\delta\hat{h}, A\epsilon\delta\hat{H})$ noting that

$$\hat{R} = 1 - \epsilon\hat{\alpha}\beta + \epsilon\hat{y}, \quad \hat{S} = \sqrt{\epsilon^2\hat{\alpha}^2 + \hat{R}^2}, \quad \text{and} \quad \hat{H} = 1. \tag{9}$$

By requiring that the pressure drives the axial velocity $\hat{u}$ at leading order and that the duct Reynolds number $\mathrm{Re}_H := \rho U A\epsilon\delta/\mu$ is large enough that the axial velocity $\hat{u}$ drives a cross-flow in $\hat{v}, \hat{w}$, it can be inferred that

$$p = \frac{\mu U}{A\epsilon^2\delta^2}\hat{p} \quad \text{and} \quad \delta\mathrm{Re}_H = O(1). \tag{10}$$

For convenience, we define the modified Reynolds number $\mathrm{Re}_\delta = \delta\mathrm{Re}_H$. Additionally, the governing equations will be expressed in terms of the modified dimensionless axial velocity component $\bar{u} := \hat{u}/\hat{S}$ (equivalently $\bar{u} = Au/U$). Again, using the microfluidic device of Warkiani *et al.*[15] as an example, one has $\epsilon = 1/80$, $\delta = 7/20$, $\hat{\alpha} = 10/3\pi$, and $\hat{h}(\hat{y}) = 1 + 5\hat{y}/21$. Additionally, given the reported throughput of 7.5 ml in 8 min of the red blood cell lysed samples through the device, we estimate Re_δ to be in the range [7.5, 15] assuming a kinematic viscosity in the range of $[1, 2]$ mm^2/s, and thus, the assumption $\mathrm{Re}_\delta = O(1)$ seems within reason.

With these scalings, we obtain the mass conservation equation

$$\frac{\partial\bar{u}}{\partial\beta} + \frac{\partial\hat{v}}{\partial\hat{y}} + \frac{\partial\hat{w}}{\partial\hat{z}} - \epsilon\frac{\hat{\alpha}}{\hat{R}}\bar{u} + \frac{\epsilon}{\hat{R}}\hat{v} = 0, \tag{11}$$

and the momentum equations

$$\begin{aligned}
&\mathrm{Re}_\delta\epsilon\left(\bar{u}\frac{\partial\bar{u}}{\partial\beta} + \hat{v}\frac{\partial\bar{u}}{\partial\hat{y}} + \hat{w}\frac{\partial\bar{u}}{\partial\hat{z}} + \frac{2\epsilon}{\hat{R}}\hat{v}\bar{u} - \frac{2\epsilon\hat{\alpha}}{\hat{R}}\bar{u}^2\right)\\
&\quad = -\frac{1}{\hat{R}^2}\frac{\partial\hat{p}}{\partial\beta} - \frac{\hat{\alpha}}{\hat{R}^2}\frac{\partial\hat{p}}{\partial\hat{y}} + \frac{\partial^2\bar{u}}{\partial\hat{z}^2} + \delta^2\frac{\hat{S}^2}{\hat{R}^2}\frac{\partial^2\bar{u}}{\partial\hat{y}^2}\\
&\qquad + \delta^2\epsilon\left(\frac{\epsilon}{\hat{R}^2}\frac{\partial^2\bar{u}}{\partial\beta^2} + \frac{2\epsilon\hat{\alpha}}{\hat{R}^2}\frac{\partial^2\bar{u}}{\partial\beta\partial\hat{y}} - \frac{2\epsilon^2\hat{\alpha}}{\hat{R}^3}\frac{\partial\bar{u}}{\partial\beta} + \frac{2\epsilon^2}{\hat{R}^3}\frac{\partial\hat{v}}{\partial\beta}\right.\\
&\qquad\quad \left. + \frac{2\epsilon^2\hat{\alpha}}{\hat{R}^3}\frac{\partial\hat{v}}{\partial\beta} + \frac{3\hat{R}^2 - 2\epsilon^2\hat{\alpha}^2}{\hat{R}^3}\frac{\partial\bar{u}}{\partial\hat{y}}\right),
\end{aligned} \tag{12a}$$

$$\begin{aligned}
&\mathrm{Re}_\delta\epsilon\left(\bar{u}\frac{\partial\hat{v}}{\partial\beta} + \hat{v}\frac{\partial\hat{v}}{\partial\hat{y}} + \hat{w}\frac{\partial\hat{v}}{\partial\hat{z}} - \frac{2\epsilon^2\hat{\alpha}^2 + \hat{R}^2}{\epsilon\hat{R}}\bar{u}^2 + \frac{2\epsilon\hat{\alpha}}{\hat{R}}\hat{v}\bar{u}\right)\\
&\quad = -\frac{\hat{\alpha}}{\hat{R}^2}\frac{\partial\hat{p}}{\partial\beta} - \frac{1}{\epsilon^2}\frac{\hat{S}^2}{\hat{R}^2}\frac{\partial\hat{p}}{\partial\hat{y}} + \frac{\partial^2\hat{v}}{\partial\hat{z}^2} + \delta^2\frac{\hat{S}^2}{\hat{R}^2}\frac{\partial^2\hat{v}}{\partial\hat{y}^2}\\
&\qquad + \epsilon\delta^2\left(\frac{\epsilon}{\hat{R}^2}\frac{\partial^2\hat{v}}{\partial\beta^2} + \frac{2\epsilon\hat{\alpha}}{\hat{R}^2}\frac{\partial^2\hat{v}}{\partial\beta\partial\hat{y}} - 2\frac{\hat{S}^2}{\hat{R}^3}\frac{\partial\bar{u}}{\partial\beta} + \frac{2\epsilon^2\hat{\alpha}}{\hat{R}^3}\frac{\partial\hat{v}}{\partial\beta}\right.\\
&\qquad\quad \left. - \frac{2\epsilon^2\hat{\alpha}^3}{\hat{R}^3}\frac{\partial\bar{u}}{\partial\hat{y}} + \frac{2\epsilon^2\hat{\alpha}^2 + \hat{R}^2}{\hat{R}^3}\frac{\partial\hat{v}}{\partial\hat{y}} + \frac{\epsilon\hat{\alpha}}{\hat{R}^2}\bar{u} - \frac{\epsilon}{\hat{R}^2}\hat{v}\right),
\end{aligned} \tag{12b}$$

$$\begin{aligned}
&\mathrm{Re}_\delta\epsilon\left(\bar{u}\frac{\partial\hat{w}}{\partial\beta} + \hat{v}\frac{\partial\hat{w}}{\partial\hat{y}} + \hat{w}\frac{\partial\hat{w}}{\partial\hat{z}}\right)\\
&\quad = -\frac{1}{\epsilon^2\delta^2}\frac{\partial\hat{p}}{\partial\hat{z}} + \frac{\partial^2\hat{w}}{\partial\hat{z}^2} + \delta^2\frac{\hat{S}^2}{\hat{R}^2}\frac{\partial^2\hat{w}}{\partial\hat{y}^2}\\
&\qquad + \epsilon\delta^2\left(\frac{\epsilon}{\hat{R}^2}\frac{\partial^2\hat{w}}{\partial\beta^2} + \frac{2\epsilon\hat{\alpha}}{\hat{R}^2}\frac{\partial^2\hat{w}}{\partial\beta\partial\hat{y}} + \frac{1}{\hat{R}}\frac{\partial\hat{w}}{\partial\hat{y}}\right).
\end{aligned} \tag{12c}$$

It will be convenient to write the mass conservation equation (11) in the alternative form

$$\frac{1}{\hat{R}}\left(\frac{\partial\hat{R}\bar{u}}{\partial\beta} + \frac{\partial\hat{R}\hat{v}}{\partial\hat{y}} + \frac{\partial\hat{R}\hat{w}}{\partial\hat{z}}\right) = 0, \tag{13}$$

from which the common factor $1/\hat{R}$ can be dropped. Examination of (12), under the assumption $\mathrm{Re}_\delta = O(1)$, suggests that a perturbation expansion of $\bar{u}, \hat{v}, \hat{w}$, and $\hat{p}$ in powers of δ^2 and ϵ is appropriate. We begin by finding the leading order solution for small ϵ and δ^2 in Sec. III and then find first-order corrections with respect to ϵ and δ^2 in Sec. IV.

III. LEADING ORDER SOLUTIONS

A. Derivation

Here we consider the leading order solution of flow through the spiral duct when both ϵ and δ^2 are assumed to be small. No additional assumptions are made regarding the relative size of ϵ and δ^2. For convenience, $\hat{R}$ is expressed as $\hat{R} = \hat{R}_0 + \epsilon\hat{y}$ (and thus $\hat{R}_0 = 1 - \epsilon\hat{\alpha}\beta$) and for small ϵ the approximation $\hat{R} \approx \hat{R}_0$ will be used. The reason for keeping the $-\epsilon\hat{\alpha}\beta$ term in $\hat{R}_0$ is that we wish to consider large β such that $\epsilon\beta = O(1)$. Similarly it is observed that $\hat{S} \approx \hat{R}_0$ for small ϵ.

Consider now a perturbation expansion of $\hat{p}, \bar{u}, \hat{v}, \hat{w}$ in powers of both ϵ and δ^2, i.e., of the general form

$$\zeta = \sum_{i=0}^{\infty}\sum_{j=0}^{\infty}\epsilon^i\delta^{2j}\zeta_{i,j}. \tag{14}$$

Substituting these expansions into the momentum equations (12) and removing all order ϵ and δ^2 terms (or smaller) lead to

$$0 = -\frac{1}{\hat{R}_0^2}\frac{\partial\hat{p}_{0,0}}{\partial\beta} - \frac{\hat{\alpha}}{\hat{R}_0^2}\frac{\partial\hat{p}_{0,0}}{\partial\hat{y}} + \frac{\partial^2\bar{u}_{0,0}}{\partial\hat{z}^2}, \tag{15a}$$

$$-\mathrm{Re}_\delta \hat{R}_0 \bar{u}_{0,0}^2 = -\frac{\hat{\alpha}}{\hat{R}_0^2}\frac{\partial \hat{p}_{0,0}}{\partial \beta} - \frac{\hat{\alpha}^2}{\hat{R}_0^2}\frac{\partial \hat{p}_{0,0}}{\partial \hat{y}} - \frac{1}{\epsilon^2}\frac{\partial \hat{p}}{\partial \hat{y}} + \frac{\partial^2 \hat{v}_{0,0}}{\partial \hat{z}^2}, \tag{15b}$$

$$0 = -\frac{1}{\epsilon^2\delta^2}\frac{\partial \hat{p}}{\partial \hat{z}} + \frac{\partial^2 \hat{w}_{0,0}}{\partial \hat{z}^2}, \tag{15c}$$

and similarly, the continuity equation can be written as

$$\frac{\partial \hat{R}_0 \bar{u}_{0,0}}{\partial \beta} + \frac{\partial \hat{R}_0 \hat{v}_{0,0}}{\partial \hat{y}} + \frac{\partial \hat{R}_0 \hat{w}_{0,0}}{\partial \hat{z}} = 0. \tag{16}$$

We refrained from substituting the expansion of $\hat{p}$ into the terms in (15a) having factors ϵ^{-2} and $\epsilon^{-2}\delta^{-2}$ as some care needs to be taken with these. Notice that the presence of these terms means that, at a minimum, $\hat{p}_{0,0}, \hat{p}_{1,0}$ are independent of $\hat{y}$ and $\hat{p}_{0,0}, \hat{p}_{1,0}, \hat{p}_{2,0}, \hat{p}_{0,1}, \hat{p}_{1,1}$ are independent of $\hat{z}$. An immediate consequence of this is that the $\partial \hat{p}_{0,0}/\partial \hat{y}$ terms can be dropped from (15). Additional terms may also be independent of $\hat{y}$, $\hat{z}$ depending on the relative magnitude of ϵ and δ^2. Specifically, if there is an integer $\ell \geq 1$ such that $\epsilon^\ell/\delta^2 = O(1)$, then one must additionally have $\hat{p}_{0,1}$ independent of $\hat{y}$ and $\hat{p}_{0,2}$ independent of $\hat{z}$, if $\ell = 1$, and $\hat{p}_{3,0}, \ldots, \hat{p}_{1+\ell,0}$ independent of $\hat{z}$ if $\ell \geq 2$. On the other hand, if there is an integer $k \geq 1$ such that $\delta^{2k}/\epsilon = O(1)$, then $\hat{p}_{0,0}, \hat{p}_{0,1}, \ldots, \hat{p}_{0,2k-1}$ and $\hat{p}_{1,0}, \hat{p}_{1,1}, \ldots, \hat{p}_{1,k-1}$ are independent of both $\hat{y}$ and $\hat{z}$, and $\hat{p}_{0,2k}, \hat{p}_{1,k}$ are independent of $\hat{z}$. It follows that, in either case, the $O(1)$ contributions to (15a) from these pressure terms are

$$\frac{1}{\epsilon^2}\frac{\partial \hat{p}}{\partial \hat{y}} \longrightarrow \frac{\partial}{\partial \hat{y}}\left(\hat{p}_{2,0} + \hat{p}_{1,k} + \hat{p}_{0,2k} + \hat{p}_{0,1}|_{\ell=2}\right), \tag{17a}$$

$$\frac{1}{\epsilon^2\delta^2}\frac{\partial \hat{p}}{\partial \hat{z}} \longrightarrow \frac{\partial}{\partial \hat{z}}\left(\hat{p}_{2,1} + \hat{p}_{1,1+k} + \hat{p}_{0,1+2k} + \hat{p}_{2+\ell,0} + \hat{p}_{0,2}|_{\ell=2}\right), \tag{17b}$$

where the terms with k, ℓ are understood to be present only if $\delta^{2k}/\epsilon = O(1)$ and $\epsilon^\ell/\delta^2 = O(1)$, respectively [with $\hat{p}_{0,1}|_{\ell=2}$ and $\hat{p}_{0,1}|_{\ell=2}$ meaning that these terms are only present when $\epsilon^2/\delta^2 = O(1)$]. Observing that the terms contributing to $\epsilon^{-2}\partial \hat{p}/\partial \hat{y}$ are independent of $\hat{z}$, we aggregate these contributions into the terms

$$\bar{p}_{2,0}(\beta, \hat{y}) = \hat{p}_{2,0} + \hat{p}_{1,k} + \hat{p}_{0,2k} + \hat{p}_{0,1}|_{\ell=2}, \tag{18a}$$

$$\bar{p}_{2,1}(\beta, \hat{y}, \hat{z}) = \hat{p}_{2,1} + \hat{p}_{1,1+k} + \hat{p}_{0,1+2k} + \hat{p}_{2+\ell,0} + \hat{p}_{0,2}|_{\ell=2}. \tag{18b}$$

With these, (15) is then expressed as

$$0 = -\frac{1}{\hat{R}_0^2}\frac{\partial \hat{p}_{0,0}}{\partial \beta} + \frac{\partial^2 \bar{u}_{0,0}}{\partial \hat{z}^2}, \tag{19a}$$

$$-\mathrm{Re}_\delta \hat{R}_0 \bar{u}_{0,0}^2 = -\frac{\hat{\alpha}}{\hat{R}_0^2}\frac{\partial \hat{p}_{0,0}}{\partial \beta} - \frac{\partial \bar{p}_{2,0}}{\partial \hat{y}} + \frac{\partial^2 \hat{v}_{0,0}}{\partial \hat{z}^2}, \tag{19b}$$

$$0 = -\frac{\partial \bar{p}_{2,1}}{\partial \hat{z}} + \frac{\partial^2 \hat{w}_{0,0}}{\partial \hat{z}^2}. \tag{19c}$$

We now proceed to solve these equations.

Since $\hat{p}_{0,0}$ is independent of $\hat{z}$, we can integrate (19a) with respect to $\hat{z}$ twice and enforce the no slip boundary condition $\bar{u}_{0,0}$ on $\hat{z} = 0, \hat{h}(\hat{y})$ to obtain

$$\bar{u}_{0,0} = \frac{1}{2\hat{R}_0^2}\frac{\partial \hat{p}_{0,0}}{\partial \beta}\hat{z}(\hat{z} - \hat{h}). \tag{20}$$

The $\partial \hat{p}_{0,0}/\partial \beta$ is determined by the assumption concerning how the flow is driven. There are two different ways we could specify $\hat{p}_{0,0}$. The first is to assume that $\hat{p}_{0,0}$ has a constant gradient (with respect to the arc-length) along the duct centre-line which is driving the axial flow. A second approach is to instead specify a fixed axial flow rate through any cross section of the spiral from which $\hat{p}_{0,0}$ is then determined. In this case, the two approaches lead to identical leading order solutions. We will apply the former here and then later determine the corresponding flow rate.

Let $\mathbf{s} := \mathbf{s}(\beta)$ be the path along the centre-line: that is, upon writing (5) in terms of the dimensionless coordinates and setting $\hat{y} = \hat{z} = 0$, we obtain $\mathbf{s} = (1 - \epsilon\hat{\alpha}\beta)(\cos(\beta)\hat{\mathbf{i}} + \sin(\beta)\hat{\mathbf{j}})$. The tangent vector to the path at a given β is given by

$$\mathbf{t}(\beta) = \frac{\partial \mathbf{s}}{\partial \beta} = (-\epsilon\hat{\alpha}\cos(\beta) - (1 - \epsilon\hat{\alpha}\beta)\sin(\beta))\hat{\mathbf{i}} + (-\epsilon\hat{\alpha}\sin(\beta) + (1 - \epsilon\hat{\alpha}\beta)\cos(\beta))\hat{\mathbf{j}}. \tag{21}$$

Upon normalising $\mathbf{t}$ as $\bar{\mathbf{t}} = \mathbf{t}/\hat{S}$, the assumption for the leading pressure term can be expressed as the directional derivative $\nabla_{\bar{\mathbf{t}}}\hat{p}_{0,0}(\mathbf{s}) = -G$, where G is a dimensionless constant denoting the pressure drop per unit arc length along the centre-line. Noting that $A\mathbf{t} = \partial \mathbf{x}/\partial \beta$, it follows that

$$-G = \nabla_{\bar{\mathbf{t}}}\hat{p}_{0,0}(\mathbf{s}) = \nabla \hat{p}_{0,0}(\mathbf{s}) \cdot \frac{\mathbf{t}}{\hat{S}} = \frac{1}{\hat{S}}\frac{\partial \hat{p}_{0,0}(\mathbf{s})}{\partial \beta}. \tag{22}$$

Thus the leading pressure term satisfies $\partial \hat{p}_{0,0}(\mathbf{s})/\partial \beta = -G\hat{S} \approx -G\hat{R}_0$ which gives

$$\bar{u}_{0,0} = \frac{G}{2\hat{R}_0}\hat{z}(\hat{h} - \hat{z}). \tag{23}$$

Before proceeding to determine $\hat{v}_{0,0}, \hat{w}_{0,0}$, the definition of the characteristic velocity U can be used to determine the value of G via $\bar{u}_{0,0}$ (neglecting contributions to $\hat{u}$ from higher order terms). The maximal value of $\bar{u}_{0,0}$ with respect to $\hat{z}$, for any $\beta, \hat{y}$, is clearly achieved at $\hat{z} = \hat{h}(\hat{y})/2$ and attains the value

$$\max_{\hat{z}} \bar{u}_{0,0} = \frac{G\hat{h}(\hat{y})^2}{8\hat{R}_0}. \tag{24}$$

At the specific coordinates $\beta = \hat{y} = 0$, where $\hat{R}_0 = 1$ and $\hat{h}(0) = \hat{H} = 1$, this reduces to

$$\max_{\hat{z}} \bar{u}_{0,0}|_{\beta=\hat{y}=0} = \frac{G}{8}. \tag{25}$$

Since the physical velocity is given by $U\bar{u}\hat{S} \to U\bar{u}_{0,0}\hat{R}_0$, then the maximal axial velocity at $\beta = \hat{y} = 0$ is

$$\max_{\hat{z}} \left(U\bar{u}_{0,0}\hat{R}_0\right)_{\beta=\hat{y}=0} = \frac{GU}{8}, \tag{26}$$

and, since this is equal to U by definition of the characteristic velocity, it follows that $G = 8$ at leading order and thus

$$\bar{u}_{0,0} = \frac{4}{\hat{R}_0}\hat{z}(\hat{h} - \hat{z}). \tag{27}$$

Now we continue to find the $\hat{v}_{0,0}, \hat{w}_{0,0}$ velocity components. Given that we have $\bar{u}_{0,0}$, then our strategy is to obtain $\hat{v}_{0,0}$ from (19b) and $\hat{w}_{0,0}$ from (16). Note that Eq. (19c) relating $\hat{w}_{0,0}$ to a small pressure term need not be used. Substituting

(27) and $\hat{p}_{0,0}$ into (19b) and integrating twice with respect to $\hat{z}$, recalling that $\bar{p}_{2,0}$ is independent of $\hat{z}$, lead to

$$\hat{v}_{0,0} = -\frac{4\hat{\alpha}}{\hat{R}_0}\hat{z}^2 + \frac{\partial \bar{p}_{2,0}}{\partial \hat{y}}\frac{\hat{z}^2}{2} - \frac{16\mathrm{Re}_\delta}{\hat{R}_0}\left(\frac{\hat{z}^6}{30} - \frac{\hat{h}\hat{z}^5}{10} + \frac{\hat{h}^2\hat{z}^4}{12}\right) + g_1(\beta,\hat{y})\hat{z} + g_0(\beta,\hat{y}), \tag{28}$$

where g_0, g_1 are chosen to satisfy the boundary conditions on $\hat{z} = 0$, $\hat{h}(\hat{y})$. Using the no slip condition $\hat{v}_{0,0} = 0$ at $\hat{z} = 0$ immediately gives $g_0 = 0$. Similarly, setting $\hat{v}_{0,0} = 0$ at $\hat{z} = \hat{h}(\hat{y})$ gives

$$g_1(\beta,\hat{y}) = \frac{4\hat{\alpha}}{\hat{R}_0}\hat{h} - \frac{\partial \hat{p}_{2,0}}{\partial \hat{y}}\frac{\hat{h}}{2} + \frac{16\mathrm{Re}_\delta}{\hat{R}_0}\frac{\hat{h}^5}{60}. \tag{29}$$

Substituting g_0 and g_1 into (28) then gives

$$\hat{v}_{0,0} = -\frac{4\hat{\alpha}}{\hat{R}_0}\hat{z}(\hat{z}-\hat{h}) + \frac{\partial \bar{p}_{2,0}}{\partial \hat{y}}\frac{\hat{z}(\hat{z}-\hat{h})}{2} - \frac{16\mathrm{Re}_\delta}{\hat{R}_0}\left(\frac{\hat{z}^6}{30} - \frac{\hat{h}\hat{z}^5}{10} + \frac{\hat{h}^2\hat{z}^4}{12} - \frac{\hat{h}^5\hat{z}}{60}\right). \tag{30}$$

In order to determine $\partial \bar{p}_{2,0}/\partial \hat{y}$, we claim that $\int_0^{\hat{h}} \hat{v}_{0,0}\, d\hat{z} = 0$. To prove this, observe that $\hat{R}_0\bar{u}_{0,0}$ is independent of β, and thus, noting that $\hat{R}_0$ does not depend on $\hat{y}$, $\hat{z}$, (16) reduces to

$$\frac{\partial \hat{v}_{0,0}}{\partial \hat{y}} + \frac{\partial \hat{w}_{0,0}}{\partial \hat{z}} = 0. \tag{31}$$

Integrating with respect to $\hat{z}$ from 0 to $\hat{h}(\hat{y})$ [applying the boundary conditions $\hat{w}_{0,0} = 0$ at $\hat{z} = 0$ and $\hat{z} = \hat{h}(\hat{y})$], we obtain

$$\int_0^{\hat{h}} \frac{\partial \hat{v}_{0,0}}{\partial \hat{y}}\, d\hat{z} = 0. \tag{32}$$

Applying the Leibniz integration rule gives

$$\int_0^{\hat{h}} \frac{\partial \hat{v}_{0,0}}{\partial \hat{y}}\, d\hat{z} = \frac{\partial}{\partial \hat{y}}\int_0^{\hat{h}} \hat{v}_{0,0}\, d\hat{z} - \hat{v}_{0,0}|_{\hat{z}=\hat{h}}\,\hat{h}'(\hat{y}) = \frac{\partial}{\partial \hat{y}}\int_0^{\hat{h}} \hat{v}_{0,0}\, dz,$$

where the last equality holds since $\hat{v}_{0,0} = 0$ when $\hat{z} = \hat{h}$. It follows that

$$\int_0^{\hat{h}} \hat{v}_{0,0}\, d\hat{z} = C, \tag{33}$$

where the constant C must be zero for the mass of fluid to be preserved in an infinitesimally thin vertical column of fluid.

With the claim verified, we apply it to determine $\partial \bar{p}_{2,0}/\partial \hat{y}$. Integrating $\hat{v}_{0,0}$ with respect to $\hat{z}$, recalling once again that $\bar{p}_{2,0}$ is independent of $\hat{z}$, yields

$$0 = \int_0^{\hat{h}} \hat{v}_{0,0}\, d\hat{z} = \frac{4\hat{\alpha}}{\hat{R}_0}\frac{\hat{h}^3}{6} - \frac{\partial \hat{p}_{2,0}}{\partial \hat{y}}\frac{\hat{h}^3}{12} + \frac{16\mathrm{Re}_\delta}{\hat{R}_0}\frac{\hat{h}^7}{280}. \tag{34}$$

Re-arranging for $\partial \hat{p}_{2,0}/\partial \hat{y}$ and then substituting into (30) lead to the solution

$$\hat{v}_{0,0} = -\frac{16\mathrm{Re}_\delta}{\hat{R}_0}\left(\frac{\hat{z}^6}{30} - \frac{\hat{h}\hat{z}^5}{10} + \frac{\hat{h}^2\hat{z}^4}{12} - \frac{3\hat{h}^4\hat{z}^2}{140} + \frac{\hat{h}^5\hat{z}}{210}\right). \tag{35}$$

Now $\hat{w}_{0,0}$ is found by substituting $\hat{v}_{0,0}$ into (31) to obtain

$$\frac{\partial \hat{w}_{0,0}}{\partial \hat{z}} = \frac{16\mathrm{Re}_\delta}{\hat{R}_0}\left(-\frac{\hat{z}^5}{10} + \frac{\hat{h}\hat{z}^4}{6} - \frac{3\hat{h}^3\hat{z}^2}{35} + \frac{\hat{h}^4\hat{z}}{42}\right)\hat{h}', \tag{36}$$

where $\hat{h}' = \hat{h}'(\hat{y}) := d\hat{h}(\hat{y})/d\hat{y}$. Integrating and enforcing the boundary condition $\hat{w}_{0,0} = 0$ at $\hat{z} = 0$ yield

$$\hat{w}_{0,0} = -\frac{16\mathrm{Re}_\delta}{\hat{R}_0}\left(\frac{z^6}{60} - \frac{\hat{z}^5\hat{h}}{30} + \frac{\hat{z}^3\hat{h}^3}{35} - \frac{\hat{z}^2\hat{h}^4}{84}\right)\hat{h}'. \tag{37}$$

B. Discussion

Note that $\bar{u}_{0,0}$, $\hat{v}_{0,0}$, $\hat{w}_{0,0}$ can be written equivalently in the factored forms

$$\bar{u}_{0,0} = \frac{4}{\hat{R}_0}\hat{h}^2\frac{\hat{z}}{\hat{h}}\left(1 - \frac{\hat{z}}{\hat{h}}\right), \tag{38a}$$

$$\hat{v}_{0,0} = \frac{4\mathrm{Re}_\delta}{105\hat{R}_0}\hat{h}^6\frac{\hat{z}}{\hat{h}}\left(1 - \frac{\hat{z}}{\hat{h}}\right)\left(14\left(\frac{\hat{z}}{\hat{h}}\right)^4 - 28\left(\frac{\hat{z}}{\hat{h}}\right)^3 + 7\left(\frac{\hat{z}}{\hat{h}}\right)^2 + 7\frac{\hat{z}}{\hat{h}} - 2\right), \tag{38b}$$

$$\hat{w}_{0,0} = \frac{4\mathrm{Re}_\delta}{105\hat{R}_0}\hat{h}^6\hat{h}'\left(\frac{\hat{z}}{\hat{h}}\right)^2\left(1 - \frac{\hat{z}}{\hat{h}}\right)\left(7\left(\frac{\hat{z}}{\hat{h}}\right)^3 - 7\left(\frac{\hat{z}}{\hat{h}}\right)^2 - 7\frac{\hat{z}}{\hat{h}} + 5\right), \tag{38c}$$

in which it is clear that the Dirichlet boundary conditions at $\hat{z} = 0$ and $\hat{z} = \hat{h}(\hat{y})$ are indeed satisfied. Furthermore, in this form, the change in magnitude of each velocity component with respect to changes in $\hat{h}$ and $\hat{h}'$ for a fixed $\hat{z}/\hat{h}$ is evident.

Observe that $\hat{v}_{0,0}$ attains a maximum with respect to $\hat{z}$ at $\hat{z} = \hat{h}/2$ with value $\mathrm{Re}_\delta\hat{h}^6/(168\hat{R}_0)$ [and also has minima at $(1 \pm \sqrt{735 - 42\sqrt{133}}/21)\hat{h}/2$ with smaller value in magnitude]; thus, at the particular location, $\beta = \hat{y} = 0$ the maximum value is $\mathrm{Re}_\delta/168$. Similarly, provided $\hat{h}'$ is non-zero, $\hat{w}_{0,0}$ has extrema with respect to $\hat{z}$ at $\hat{z} \approx 0.33\,729\hat{h}$, $0.813\,097\hat{h}$ attaining values of approximately $1.0187\mathrm{Re}_\delta\hat{h}^6\hat{h}'/(168\hat{R}_0)$, $-1.2310\mathrm{Re}_\delta\hat{h}^6\hat{h}'/(168\hat{R}_0)$, respectively. From this, it is evident that $\bar{u}_{0,0}$, $168\hat{v}_{0,0}/\mathrm{Re}_\delta$, and $168\hat{w}_{0,0}/\mathrm{Re}_\delta$ are all of similar magnitude near $\hat{y} = \beta = 0$ [albeit with $168\hat{w}_{0,0}/\mathrm{Re}_\delta$ generally smaller on account of $\hat{h}'(0)$ expected to be small] which validates the scaling arguments which lead to Eqs. (19).

We end this discussion by determining the relation between the characteristic velocity U and a physical pressure which drives the flow. Consider a pressure P_{in} applied to the inlet of the spiral compared to some pressure P_{out} (e.g., atmospheric pressure) at the outlet, where the total spiral angle is $\beta_{\max}$. Let $-\Delta P$ denote the average (dimensional) pressure change per unit arc-length over the centre-line, that is, $-\Delta P = (P_{\mathrm{out}} - P_{\mathrm{in}})/L$, where L is the length of the spiral measured along the centre-line ($\hat{y} = \hat{z} = 0$). Noting that physical arc-length s along the centre-line is given by

$$s = \int_0^{\beta} \sqrt{\alpha^2 + (A - \alpha\beta')^2}\, d\beta', \tag{39}$$

then the pressure assumption is expressed as

$$\frac{\partial p}{\partial \beta} = -\Delta P\frac{ds}{d\beta} = -\Delta P\sqrt{\alpha^2 + (A - \alpha\beta)^2} = -\Delta P A\hat{S}|_{\hat{y}=0}.$$

Therefore, since $\hat{S}|_{y=0} \sim \hat{R}_0$ for vanishing ϵ, the leading order dimensionless pressure satisfies

$$-\Delta P A \hat{R}_0 \approx \frac{\mu U}{A\epsilon^2\delta^2}\frac{\partial \hat{p}}{\partial \beta} \approx \frac{\mu U}{A\epsilon^2\delta^2}\frac{\partial \hat{p}_{0,0}}{\partial \beta} = \frac{\mu U}{A\epsilon^2\delta^2}(-G\hat{R}_0). \tag{40}$$

Thus, equating the left and right most terms and substituting $G = 8$, we conclude that

$$\Delta P = \frac{8\mu U}{A^2\epsilon^2\delta^2}, \quad \text{or equivalently,} \quad U = \frac{A^2\epsilon^2\delta^2\Delta P}{8\mu}. \tag{41}$$

Similarly, the modified Reynolds number can be expressed in terms of ΔP, specifically

$$\mathrm{Re}_\delta = \frac{\rho U A \epsilon \delta^2}{\mu} = \frac{\rho \Delta P A^3 \epsilon^3 \delta^4}{8\mu^2}. \tag{42}$$

Thus, given specific values of ρ and μ for the fluid, the system is completely determined by ΔP. Note that these quantities can also be expressed in terms of the characteristic height and half-width of the duct as $U = \Delta P H^2/8\mu$ and $\mathrm{Re} = \rho \Delta P H^4/(8a\mu^2)$.

Alternatively we can specify the system in terms of an axial flow rate. Let the (physical) flux through a cross section of the spiral at a particular β be given by

$$Q(\beta) \coloneqq \int_{-a}^{a}\int_0^{h(y)} Su\, dz\, dy. \tag{43}$$

Noting that $Su = U\hat{S}\bar{u} \sim U\hat{R}_0\bar{u}_{0,0}$, it follows that

$$\begin{aligned} Q(\beta) &= A^2\epsilon^2\delta \int_{-1}^{1}\int_0^{\hat{h}(\hat{y})} 4U\hat{z}(\hat{h}-\hat{z})\, d\hat{z}\, d\hat{y} \\ &= \frac{2}{3}UA^2\epsilon^2\delta\int_{-1}^{1}\hat{h}(\hat{y})^3\, d\hat{y}. \end{aligned} \tag{44}$$

Observe that the right-hand side is independent of β (as was claimed prior to specifying $\partial\hat{p}_{0,0}/\partial\beta$) such that we may write $Q(\beta) = Q$ and our system can be completely determined by Q via

$$U = \frac{3Q}{2aH}\Big/\int_{-1}^{1}\hat{h}(\hat{y})^3\, d\hat{y}. \tag{45}$$

It is important to point out that Q as given in (44) will generally be an over-estimate of the true flux because $\bar{u}_{0,0}$ does not go to zero at $\hat{y} = \pm 1$. The corrections near the boundary are discussed in Sec. V, and the flux is easily adjusted based upon the corrections derived therein.

IV. FIRST-ORDER CORRECTIONS

The goal of this section is to find the first-order corrections to $\bar{u}, \hat{v}, \hat{w}$ with respect to both ϵ and δ^2, i.e., we solve for $\bar{u}_{1,0}$, $\bar{u}_{0,1}$ and similar for $\hat{v}, \hat{w}$. In obtaining the first-order corrections with respect to ϵ, we may assume that $\delta^2 \ll \epsilon$ and vice versa. The two corrections obtained in this way provide a (multi-)linear approximation of the flow when expressed as a multinomial expansion in ϵ and δ^2. In the case that $\delta^2 \sim \epsilon$, and more generally, the two corrections can be added to obtain a complete first-order approximation of the flow solution.

A. The order δ^2 correction when $\epsilon \ll \delta^2$

The $O(\delta^2)$ corrections $\bar{u}_{0,1}, \hat{v}_{0,1}, \hat{w}_{0,1}$ will be determined under the assumption that ϵ is much smaller than δ^2. Removing all $O(\epsilon)$ or smaller terms from the momentum equations (12), substituting the perturbation expansion (14) for $\hat{p}, \bar{u}, \hat{v}, \hat{w}$, and eliminating the leading order terms, we obtain the $O(\delta^2)$ equations

$$0 = \frac{\partial \hat{R}_0\bar{u}_{0,1}}{\partial\beta} + \frac{\partial \hat{R}_0\hat{v}_{0,1}}{\partial\hat{y}} + \frac{\partial \hat{R}_0\hat{w}_{0,1}}{\partial\hat{z}}, \tag{46a}$$

$$0 = -\frac{1}{\hat{R}_0^2}\frac{\partial\hat{p}_{0,1}}{\partial\beta} + \frac{\partial^2\bar{u}_{0,1}}{\partial\hat{z}^2} + \frac{\partial^2\bar{u}_{0,0}}{\partial\hat{y}^2}, \tag{46b}$$

$$-2\mathrm{Re}_\delta\hat{R}_0\bar{u}_{0,0}\bar{u}_{0,1} = -\frac{\hat{\alpha}}{\hat{R}_0^2}\frac{\partial\hat{p}_{0,1}}{\partial\beta} - \frac{\partial\bar{p}_{2,1}}{\partial\hat{y}} + \frac{\partial^2\hat{v}_{0,1}}{\partial\hat{z}^2} + \frac{\partial^2\hat{v}_{0,0}}{\partial\hat{y}^2}, \tag{46c}$$

$$0 = -\frac{\partial\bar{p}_{2,2}}{\partial\hat{z}} + \frac{\partial^2\hat{w}_{0,1}}{\partial\hat{z}^2} + \frac{\partial^2\hat{w}_{0,0}}{\partial\hat{y}^2}. \tag{46d}$$

Note that treatment of pressure terms is similar to that in Sec. III, in particular, $\bar{p}_{2,1}$ is as in (18b), whilst $\bar{p}_{2,2}$ is a similar aggregation of pressure terms that contribute to $\epsilon^{-2}\delta^{-2}\partial\hat{p}/\partial\hat{z}$ at order δ^2.

A strategy similar to that used in Sec. III is then used to solve (46). The pressure term $\hat{p}_{0,1}$ is independent of z and is chosen such that $\bar{u}_{0,1}$ has zero net contribution to the axial flux in any cross section. This leads to $\partial\hat{p}_{0,1}/\partial\beta = 2\hat{R}_0 b$, where

$$b = \int_{-1}^{1}\hat{h}^4\hat{h}''\, d\hat{y}\Big/\int_{-1}^{1}\hat{h}^3\, d\hat{y}, \tag{47}$$

and the solution

$$\bar{u}_{0,1} = \frac{1}{3\hat{R}_0}\hat{z}(\hat{h}-\hat{z})\left(2\hat{h}''(\hat{h}+\hat{z}) - 3b\right). \tag{48}$$

To solve for $\hat{v}_{0,1}$, first observe that from (19c) and (31) we have

$$\begin{aligned} \frac{\partial\bar{p}_{2,1}}{\partial\hat{y}} &= \frac{\partial}{\partial\hat{y}}\left(\frac{\partial\hat{w}_{0,0}}{\partial\hat{z}} + g_3(\beta,\hat{y})\right) \\ &= \frac{\partial}{\partial\hat{y}}\left(-\frac{\partial\hat{v}_{0,0}}{\partial\hat{y}} + g_3(\beta,\hat{y})\right), \end{aligned}$$

where $g_3(\beta,\hat{y})$ is obtained from integrating (19c). It is then a matter of integrating (46c) twice with respect to $\hat{z}$ ensuring $\hat{v} = 0$ on $\hat{z} = 0, \hat{h}$ (using the known $\bar{u}_{0,0}, \bar{u}_{0,1}, \hat{v}_{0,0}$) and then finding g_3 such that $\int_0^{\hat{h}}\hat{v}_{0,1}\, d\hat{z} = 0$ (shown analogous to $\int_0^{\hat{h}}\hat{v}_{0,0}\, d\hat{z} = 0$), from which one obtains

$$\begin{aligned} \hat{v}_{0,1} = \frac{2\mathrm{Re}_\delta}{1575\hat{R}_0}\hat{z}(\hat{h}-\hat{z})\Big(&-15b\left(14\hat{z}^4 - 28\hat{z}^3\hat{h}\right. \\ &\left. + 7\hat{z}^2\hat{h}^2 + 7\hat{z}\hat{h}^3 - 2\hat{h}^4\right) - 4(\hat{h}')^2\left(35\hat{z}^4 + 35\hat{z}^3\hat{h}\right. \\ &\left. - 100\hat{z}^2\hat{h}^2 + 18\hat{h}^4\right) + 2\hat{h}''\left(80\hat{z}^5 - 60\hat{z}^4\hat{h} - 165\hat{z}^3\hat{h}^2\right. \\ &\left. + 100\hat{z}^2\hat{h}^3 + 50\hat{z}\hat{h}^4 - 22\hat{h}^5\right)\Big). \end{aligned} \tag{49}$$

From here, it is straightforward to find $\hat{w}_{0,1}$ via (46a), in particular,

$$\begin{aligned} \hat{w}_{0,1} = \frac{-2\mathrm{Re}_\delta}{1575\hat{R}_0}\hat{z}^2(\hat{h}-\hat{z})\Big(&15b\hat{h}'(7\hat{z}^3 - 7\hat{z}^2\hat{h} - 7\hat{z}\hat{h}^2 + 5\hat{h}^3) \\ &+ 12(\hat{h}')^3\hat{h}(18\hat{z}^2 - 7\hat{z}\hat{h} - 15\hat{h}^2) \\ &- 2\hat{h}'\hat{h}''(40\hat{z}^4 + 75\hat{z}^3\hat{h} - 192\hat{z}^2\hat{h}^2 - 42\hat{z}\hat{h}^3 + 102\hat{h}^4) \\ &- \hat{h}'''(\hat{h}-\hat{z})(20\hat{z}^4 - 55\hat{z}^2\hat{h}^2 - 4\hat{z}\hat{h}^3 + 22\hat{h}^4)\Big). \end{aligned} \tag{50}$$

B. The order ϵ correction when $\delta^2 \ll \epsilon$

The $O(\epsilon)$ corrections $\bar{u}_{1,0}, \hat{v}_{1,0}, \hat{w}_{1,0}$ will be determined under the assumption that δ^2 is much smaller than ϵ. Removing all $O(\delta^2)$ or smaller components from (12), substituting the perturbation expansion (14) for $\hat{p}, \bar{u}, \hat{v}, \hat{w}$, and eliminating the leading order solutions, we obtain the $O(\epsilon)$ equations

$$\frac{\partial \hat{R}_0 \bar{u}_{1,0}}{\partial \beta} + \frac{\partial \hat{R}_0 \hat{v}_{1,0}}{\partial \hat{y}} + \frac{\partial \hat{R}_0 \hat{w}_{1,0}}{\partial \hat{z}} + \frac{\partial \hat{y} \bar{u}_{0,0}}{\partial \beta} + \frac{\partial \hat{y} \hat{v}_{0,0}}{\partial \hat{y}} + \frac{\partial \hat{y} \hat{w}_{0,0}}{\partial \hat{z}} = 0, \tag{51a}$$

$$\mathrm{Re}_\delta \left(\bar{u}_{0,0} \frac{\partial \bar{u}_{0,0}}{\partial \beta} + \hat{v}_{0,0} \frac{\partial \bar{u}_{0,0}}{\partial \hat{y}} + \hat{w}_{0,0} \frac{\partial \bar{u}_{0,0}}{\partial \hat{z}} \right) = -\frac{1}{\hat{R}_0^2} \frac{\partial \hat{p}_{1,0}}{\partial \beta} + \frac{\partial^2 \bar{u}_{1,0}}{\partial \hat{z}^2} + \frac{2\hat{y}}{\hat{R}_0} \frac{\partial^2 \bar{u}_{0,0}}{\partial \hat{z}^2}, \tag{51b}$$

$$\mathrm{Re}_\delta \left(\bar{u}_{0,0} \frac{\partial \hat{v}_{0,0}}{\partial \beta} + \hat{v}_{0,0} \frac{\partial \hat{v}_{0,0}}{\partial \hat{y}} + \hat{w}_{0,0} \frac{\partial \hat{v}_{0,0}}{\partial \hat{z}} - 2\hat{R}_0 \bar{u}_{0,0} \bar{u}_{1,0} - 3\hat{y} (\bar{u}_{0,0})^2 \right) = -\frac{\hat{\alpha}}{\hat{R}_0^2} \frac{\partial \hat{p}_{1,0}}{\partial \beta} - \frac{\partial \bar{p}_{3,0}}{\partial \hat{y}} - \frac{2\hat{y}}{\hat{R}_0} \frac{\partial \hat{p}_{2,0}}{\partial \hat{y}} + \frac{\partial^2 \hat{v}_{1,0}}{\partial \hat{z}^2} + \frac{2\hat{y}}{\hat{R}_0} \frac{\partial^2 \hat{v}_{0,0}}{\partial \hat{z}^2}, \tag{51c}$$

$$\mathrm{Re}_\delta \left(\bar{u}_{0,0} \frac{\partial \hat{w}_{0,0}}{\partial \beta} + \hat{v}_{0,0} \frac{\partial \hat{w}_{0,0}}{\partial \hat{y}} + \hat{w}_{0,0} \frac{\partial \hat{w}_{0,0}}{\partial \hat{z}} \right) = -\frac{\partial \bar{p}_{3,1}}{\partial \hat{z}} + \frac{\partial^2 \hat{w}_{1,0}}{\partial \hat{z}^2}. \tag{51d}$$

The pressure terms $\bar{p}_{3,0}, \bar{p}_{3,1}$ are aggregations similar to those in Secs. III A and IV A. Additionally, it can be shown that $\partial \bar{u}_{0,0}/\partial\beta$, $\partial \hat{v}_{0,0}/\partial\beta$, $\partial \hat{w}_{0,0}/\partial\beta$ are all order ϵ and therefore these contributions to the inertial terms in (51) are neglected.

The strategy for solving these equations is similar to that used to obtain the $O(\delta^2)$ corrections. Substituting known quantities into (51b) and integrating twice with respect to $\hat{z}$ (ensuring $\bar{u}_{1,0} = 0$ on $\hat{z} = 0, \hat{h}$) give

$$\bar{u}_{1,0} = \left(\frac{1}{\hat{R}_0^2} \frac{\partial \hat{p}_{1,0}}{\partial \beta} + \frac{16\hat{y}}{\hat{R}_0^2} \right) \frac{\hat{z}}{2} (\hat{z} - \hat{h}) - \frac{2\mathrm{Re}_\delta^2}{525 \hat{R}_0^2} \hat{h} \hat{h}' \hat{z} (\hat{h} - \hat{z}) \times (5\hat{z}^6 - 15\hat{z}^5 \hat{h} + 17\hat{z}^4 \hat{h}^2 - 9\hat{z}^3 \hat{h}^3 + \hat{z}^2 \hat{h}^4 + \hat{z} \hat{h}^5 + \hat{h}^6), \tag{52}$$

where $\hat{p}_{1,0}$ is specified so that $\bar{u}_{1,0}$ has zero contribution to the total axial flux in any cross section, in particular, we find $\partial \hat{p}_{1,0}/\partial\beta = c$, where

$$c = \left(\int_{-1}^{1} -\frac{104 \mathrm{Re}_\delta^2 \hat{h}' \hat{h}^{10}}{11\,025} - 16\hat{y}\hat{h}^3 \, d\hat{y} \right) \left(\int_{-1}^{1} \hat{h}^3 \, d\hat{y} \right)^{-1}. \tag{53}$$

Proceeding to find $\hat{v}_{1,0}$, all known quantities are substituted into (51c) which is then integrated twice with respect to $\hat{z}$ (ensuring $\hat{v}_{1,0} = 0$ on $\hat{z} = 0, \hat{h}$) and subsequently $\bar{p}_{0,3}$ is determined such that $\int_0^{\hat{h}} \hat{v}_{1,0} \, d\hat{z} = 0$. Subsequently, $\hat{w}_{1,0}$ is found via (51a) [with the $\bar{u}$ contributions neglected since they are $O(\epsilon)$]. We obtain

$$\begin{aligned} \hat{v}_{1,0} = {} & \frac{\mathrm{Re}_\delta}{105 \hat{R}_0^2} (c + 12\hat{y}) \hat{z} (\hat{z} - \hat{h}) (14\hat{z}^4 - 28\hat{z}^3 \hat{h} + 7\hat{z}^2 \hat{h}^2 + 7\hat{z}\hat{h}^3 - 2\hat{h}^4) + \frac{4\mathrm{Re}_\delta^3 \hat{h} \hat{h}'}{496\,621\,125 \hat{R}_0^2} \hat{z} (\hat{z} - \hat{h}) (277\,095\hat{z}^{10} \\ & - 1\,385\,475\hat{z}^9 \hat{h} + 2\,790\,697\hat{z}^8 \hat{h}^2 - 2\,849\,938\hat{z}^7 \hat{h}^3 + 1\,519\,427\hat{z}^6 \hat{h}^4 - 402\,493\hat{z}^5 \hat{h}^5 \\ & + 246\,155\hat{z}^4 \hat{h}^6 - 375\,466\hat{z}^3 \hat{h}^7 + 89\,999\hat{z}^2 \hat{h}^8 + 89\,999\hat{z}\hat{h}^9 - 25\,471\hat{h}^{10}), \end{aligned} \tag{54}$$

$$\begin{aligned} \hat{w}_{1,0} = {} & \frac{\mathrm{Re}_\delta \hat{z}^2 (\hat{z} - \hat{h})}{\hat{R}_0^2} \Bigg[\frac{\hat{h}'}{105} (c + 12\hat{y}) (7\hat{z}^3 - 7\hat{z}^2 \hat{h} - 7\hat{z}\hat{h}^2 + 5\hat{h}^3) - \frac{8}{105} (\hat{z} - \hat{h}) (2\hat{z} - \hat{h}) (\hat{z}^2 - \hat{z}\hat{h} - \hat{h}^2) \\ & - \frac{2\mathrm{Re}_\delta^2 (\hat{z} - \hat{h})}{496\,621\,125} (2\hat{z} - \hat{h}) \hat{h} \hat{h}'' (21\,315\hat{z}^8 - 85\,260\hat{z}^7 \hat{h} + 123\,872\hat{z}^6 \hat{h}^2 - 73\,206\hat{z}^5 \hat{h}^3 \\ & + 12\,096\hat{z}^4 \hat{h}^4 - 1652\hat{z}^3 \hat{h}^5 + 27\,739\hat{z}^2 \hat{h}^6 - 24\,904\hat{z}\hat{h}^7 - 25\,471\hat{h}^8) \\ & - \frac{4\mathrm{Re}_\delta^2 (\hat{h}')^2}{496\,621\,125} (21\,315\hat{z}^{10} - 255\,780\hat{z}^9 \hat{h} + 883\,176\hat{z}^8 \hat{h}^2 - 1\,373\,078\hat{z}^7 \hat{h}^3 + 1\,054\,347\hat{z}^6 \hat{h}^4 \\ & - 387\,093\hat{z}^5 \hat{h}^5 + 261\,555\hat{z}^4 \hat{h}^6 - 567\,273\hat{z}^3 \hat{h}^7 + 270\,564\hat{z}^2 \hat{h}^8 + 270\,564\hat{z}\hat{h}^9 - 152\,826\hat{h}^{10}) \Bigg]. \end{aligned} \tag{55}$$

V. BOUNDARY CORRECTIONS (NEAR $\hat{y} = \pm 1$)

The leading order solution and first-order corrections derived in Secs. III and IV do not satisfy no-slip/penetration boundary conditions on $\hat{y} = \pm 1$. Here we outline how to obtain approximate corrections of the leading order solution near the boundaries $\hat{y} = \pm 1$ at a fixed β under the assumption $\epsilon \ll \delta \ll 1$. Without loss of generality, the $\hat{y} = -1$ boundary is considered, noting that the $\hat{y} = 1$ boundary will be similar (the main difference being the inertia of the fluid is directed away from the side wall at $\hat{y} = -1$ and toward the side wall at $\hat{y} = 1$, but otherwise the equations and construction of series approximation are the same).

We introduce the new spatial variable $\hat{y} = -1 + \delta\tilde{y}$, velocity variables $\tilde{u} = \bar{u} - \bar{u}_{0,0}$, $\tilde{v} = \hat{v} - \hat{v}_{0,0}$, $\tilde{w} = \delta(\hat{w} - \hat{w}_{0,0})$, and pressure variable $\tilde{p} = \hat{p} - \hat{p}_{0,0}$. Notice that $\tilde{y}, \hat{z}$ now have the same scaling relative to the dimensional spatial coordinates, and similarly, $\tilde{v}, \tilde{w}$ also have the same scaling relative to the dimensional velocity components. Since the decay in fluid velocity near the side walls occurs over a length proportional to the duct height, this new scale allows us to capture the proper behaviour in this region. Upon substituting these into (12), neglecting terms of order ϵ or smaller [including $O(\epsilon/\delta)$ terms that appear in the inertial part], one obtains the reduced system of equations

$$0 = \frac{1}{\hat{R}_0}\frac{\partial \hat{R}_0\tilde{u}}{\partial\beta} + \frac{1}{\delta}\frac{\partial\tilde{v}}{\partial\tilde{y}} + \frac{1}{\delta}\frac{\partial\tilde{w}}{\partial\hat{z}}, \tag{56a}$$

$$0 = -\frac{1}{\hat{R}_0^2}\frac{\partial\tilde{p}}{\partial\beta} - \frac{\hat{\alpha}}{\delta\hat{R}_0^2}\frac{\partial\tilde{p}}{\partial\tilde{y}} + \frac{\partial^2\tilde{u}}{\partial\hat{z}^2} + \frac{\partial^2\tilde{u}}{\partial\tilde{y}^2}, \tag{56b}$$

$$-\mathrm{Re}_\delta\hat{R}_0(\tilde{u}^2 + 2\tilde{u}\bar{u}_{0,0}) = -\frac{\hat{\alpha}}{\hat{R}_0^2}\frac{\partial\tilde{p}}{\partial\beta} - \frac{\hat{R}_0^2 + \epsilon^2\hat{\alpha}^2}{\delta\epsilon^2\hat{R}_0^2}\frac{\partial\tilde{p}}{\partial\tilde{y}} + \frac{\partial^2\tilde{v}}{\partial\hat{z}^2} + \frac{\partial^2\tilde{v}}{\partial\tilde{y}^2}, \tag{56c}$$

$$0 = -\frac{1}{\epsilon^2\delta}\frac{\partial\tilde{p}}{\partial\hat{z}} + \frac{\partial^2\tilde{w}}{\partial\hat{z}^2} + \frac{\partial^2\tilde{w}}{\partial\tilde{y}^2}. \tag{56d}$$

Consider first the correction term $\tilde{u}$ in a neighbourhood of the boundary which is governed by equation (56b) with the boundary conditions $\tilde{u} = -\bar{u}_{0,0}$ on $\tilde{y} = 0$ (equivalently $\hat{y} = -1$), $\tilde{u} = 0$ on $\hat{z} = 0$, $\hat{h}$ [noting $\hat{h}(\hat{y}) = \hat{h}(-1 + \delta\tilde{y})$], and $\tilde{u} = 0$ on $\tilde{y} = 2/\delta$ (equivalently $\hat{y} = 1$). Note that we set $\tilde{u} = 0$ for the latter boundary condition since the correction near this wall is considered separately. Furthermore, given the assumption that δ is small, we may neglect the effect of the side wall at $\hat{y} = 1$ when constructing the correction at $\hat{y} = -1$ (and vice versa), and thus, the boundary condition $\tilde{u} = 0$ on $\tilde{y} = 2/\delta$ can be replaced by the decay condition $\tilde{u} \to 0$ as $\tilde{y} \to \infty$ (effectively treating the domain as a semi-infinite strip). We assume that the pressure which drives the flow in the central region is not significantly different in a neighbourhood of the side walls. As such, we take $\partial\tilde{p}/\partial\beta$ and $\partial\tilde{p}/\partial\tilde{y}$ to be order ϵ and $\epsilon\delta$ in magnitude, respectively, such that Eq. (56b) can now be approximated by the Laplace equation

$$0 = \frac{\partial^2\tilde{u}}{\partial\hat{z}^2} + \frac{\partial^2\tilde{u}}{\partial\tilde{y}^2}. \tag{57}$$

These assumptions have two consequences on the remaining equations in (56). First, we observe that the solution to (57) with boundary conditions as described above will be such that $\hat{R}_0\tilde{u}$ is independent of β, and therefore, the first term in Eq. (56a) can be eliminated. Second, the only pressure term of significance in (56c) is $1/(\delta\epsilon^2)\partial\tilde{p}/\partial\tilde{y}$. Therefore, $\tilde{v}, \tilde{w}$ are governed by

$$0 = \frac{\partial\tilde{v}}{\partial\tilde{y}} + \frac{\partial\tilde{w}}{\partial\hat{z}}, \tag{58a}$$

$$-\mathrm{Re}_\delta\hat{R}_0(\tilde{u}^2 + 2\tilde{u}\bar{u}_{0,0}) = -\frac{1}{\delta\epsilon^2}\frac{\partial\tilde{p}}{\partial\tilde{y}} + \frac{\partial^2\tilde{v}}{\partial\hat{z}^2} + \frac{\partial^2\tilde{v}}{\partial\tilde{y}^2}, \tag{58b}$$

$$0 = -\frac{1}{\epsilon^2\delta}\frac{\partial\tilde{p}}{\partial\hat{z}} + \frac{\partial^2\tilde{w}}{\partial\hat{z}^2} + \frac{\partial^2\tilde{w}}{\partial\tilde{y}^2}. \tag{58c}$$

The boundary conditions for $\tilde{v}, \tilde{w}$ are $\tilde{v} = -\hat{v}_{0,0}$, $\tilde{w} = -\delta\hat{w}_{0,0}$ on $\tilde{y} = 0$, $\tilde{v} = \tilde{w} = 0$ on $\hat{z} = 0, \tilde{h}$, and $\tilde{v} = \tilde{w} = 0$ on $\tilde{y} = 2/\delta$.

Since $\tilde{u}$ can be solved independently of $\tilde{v}, \tilde{w}$ (which depend on $\tilde{u}$), we consider the solution of $\tilde{u}$ first. If $\hat{h}$ is constant (such that the cross section is rectangular), then obtaining a series solution via the Fourier method is straightforward. For general $\hat{h}$, however, this is more difficult. To maintain the simplicity of our solutions, we will take the approach of solving for $\tilde{u}$ as if the domain is rectangular and then "stretching" this solution onto the actual domain: that is, letting $\tilde{u}^{\mathrm{flat}}(\tilde{y}, \hat{z})$ denote the solution assuming that $\hat{h}$ is equal to $\hat{h}(-1)$ everywhere, we take

$$\tilde{u}(\tilde{y}, \hat{z}) \approx \tilde{u}^{\mathrm{flat}}(\tilde{y}, \hat{z}\hat{h}(-1)/\hat{h}(-1 + \delta\tilde{y})). \tag{59}$$

This approximation is justified since $\tilde{u}$ decays rapidly away from $\tilde{y} = 0$ and the residual near the wall is also small as a consequence of $\partial\hat{h}/\partial\tilde{y} = \delta\hat{h}'(-1 + \delta\tilde{y})$ (recalling $\delta \ll 1$ and noting that $\hat{h}'$ is generally expected to be small since the height should not vary rapidly). For $\tilde{u}^{\mathrm{flat}}$, it is straightforward to obtain the series solution

$$\tilde{u}^{\mathrm{flat}} = \sum_{n=1}^{\infty} c_n \sin(n\pi\hat{z}/\hat{h}(-1))e^{-n\pi\tilde{y}/\hat{h}(-1)}, \tag{60}$$

where

$$c_n = \frac{-16\hat{h}(-1)^2(1 - (-1)^n)}{\hat{R}_0\pi^3 n^3}. \tag{61}$$

The final form of the correction near the left boundary is then

$$\tilde{u}(\tilde{y}, \hat{z}) \approx \sum_{n=1}^{\infty} c_n \sin\left(\frac{n\pi\hat{z}}{\hat{h}(-1 + \delta\tilde{y})}\right) e^{-n\pi\tilde{y}/\hat{h}(-1)}. \tag{62}$$

In practice we truncate the sum since the c_n decay rapidly. In our results we found that using the first 16 non-zero modes was sufficient to satisfy the boundary conditions to at least 3 decimal places for each of the examples considered. Note how the height at $\hat{y} = -1$ modifies the rate of decay of each mode of the correction; the smaller the height the quicker the rate of decay. This illustrates why the correction is constructed separately at $\hat{y} = 1$ since the height, and therefore the rate of decay near the side wall, may differ.

With these boundary corrections to $\bar{u}$, it is straightforward to obtain a correction to the flux Q through any cross section by adding the contribution of $\delta\int\int\tilde{u}\,d\tilde{y}\,d\hat{z}$ to (44). The correction of $\bar{u}$ near the boundaries can also be extended to include the first-order correction terms in ϵ and δ by simply replacing the $\bar{u}_{0,0}$ in (61) with $\bar{u}_{0,0} + \epsilon\bar{u}_{1,0} + \delta^2\bar{u}_{0,1}$. Whilst this approach correctly gives $\tilde{u} = -(\bar{u}_{0,0} + \epsilon\bar{u}_{1,0} + \delta^2\bar{u}_{0,1})$ at

$\tilde{y} = 0$, it would essentially ignore the contribution of some fluid inertia in a neighbourhood of the boundaries, specifically the terms that scale with Re_δ in (51b), but this seems reasonable to neglect given the localised nature of the correction when δ is small.

We now consider the solution of $\tilde{v}, \tilde{w}$. Notice that (58a) allows us to define a streamfunction $\tilde{\Phi}$ for which $\partial\tilde{\Phi}/\partial\tilde{y} = \tilde{w}$ and $\partial\tilde{\Phi}/\partial\hat{z} = -\tilde{v}$. Substituting this into Eqs. (58b) and (58c), the pressure term can be eliminated [i.e., by taking $\partial/\partial\tilde{y}$ of (58c) and $\partial/\partial\hat{z}$ of (58b) and then subtracting the latter from the former] to obtain the inhomogeneous biharmonic equation

$$2\mathrm{Re}_\delta \hat{R}_0 \left(\tilde{u}\frac{\partial\tilde{u}}{\partial\hat{z}} + \bar{u}_{0,0}\frac{\partial\tilde{u}}{\partial\hat{z}} + \tilde{u}\frac{\partial\bar{u}_{0,0}}{\partial\hat{z}}\right) = \left(\frac{\partial^2}{\partial\tilde{y}^2} + \frac{\partial^2}{\partial\hat{z}^2}\right)^2 \tilde{\Phi}. \quad (63)$$

The boundary conditions for $\tilde{\Phi}$ are inherited from $\tilde{v}, \tilde{w}$ and are $\tilde{\Phi} = \partial\tilde{\Phi}/\partial\hat{z} = 0$ on $\hat{z} = 0$, $\hat{h}$, $\partial\tilde{\Phi}/\partial\tilde{y} = -\hat{w}_{0,0}$ and $\partial\tilde{\Phi}/\partial\hat{z} = -\hat{v}_{0,0}$ on $\tilde{y} = 0$, and $\tilde{\Phi} = \partial\tilde{\Phi}/\partial\hat{z} = 0$ on $\tilde{y} = 2/\delta$. The boundary conditions at $\tilde{y} = 0$ can be alternatively expressed as $\tilde{\Phi} = -\hat{\Phi}_{0,0}$ and $\partial\tilde{\Phi}/\partial\tilde{y} = -\partial\hat{\Phi}_{0,0}/\partial\tilde{y}$, where $\hat{\Phi}_{0,0} := -\int \hat{v}_{0,0}\, d\hat{z}$, or equivalently,

$$\hat{\Phi}_{0,0} = \frac{16\mathrm{Re}_\delta}{\hat{R}_0}\left(\frac{\hat{z}^7}{210} - \frac{\hat{h}\hat{z}^6}{60} + \frac{\hat{h}^2\hat{z}^5}{60} - \frac{\hat{h}^4\hat{z}^3}{140} + \frac{\hat{h}^5\hat{z}^2}{420}\right), \quad (64)$$

for which it is readily checked that $\partial\hat{\Phi}_{0,0}/\partial\hat{y} = \hat{w}_{0,0}$ (thus, $\hat{\Phi}_{0,0}$ is a stream-function for the leading order solution in the central region).

Similar to $\tilde{u}$, we develop a correction $\tilde{\Phi}^{\mathrm{flat}}$ under the assumption that $\hat{h} = \hat{h}(-1)$ over the entire domain and then use the approximation

$$\tilde{\Phi}(\tilde{y}, \hat{z}) \approx \tilde{\Phi}^{\mathrm{flat}}(\tilde{y}, \hat{z}\hat{h}(-1)/\hat{h}(-1 + \delta\tilde{y})). \quad (65)$$

For $\tilde{\Phi}^{\mathrm{flat}}$, we seek a series solution of the form

$$\tilde{\Phi}^{\mathrm{flat}} = \sum_n Z_n^o(\hat{z})Y_n^o(\tilde{y}) + Z_n^e(\hat{z})Y_n^e(\tilde{y}),$$

where Z_n^o, Z_n^e are variants of Papkovich–Fadle eigenfunctions,[44] specifically

$$Z_n^o(\hat{z}) = \sin\left(\sqrt{2}\lambda_n^o\frac{2\hat{z} - \hat{h}(-1)}{\hat{h}(-1)}\right) - \frac{2\hat{z} - \hat{h}(-1)}{\hat{h}(-1)}\sin(\sqrt{2}\lambda_n^o),$$

$$Z_n^e(\hat{z}) = \cos\left(\sqrt{2}\lambda_n^e\frac{2\hat{z} - \hat{h}(-1)}{\hat{h}(-1)}\right) - \cos(\sqrt{2}\lambda_n^e),$$

with eigenvalues $\lambda_n^e = n\pi/\sqrt{2}$ and λ_n^o which is the nth solution to $\sqrt{2}\lambda = \tan(\sqrt{2}\lambda)$ (in increasing order with $\lambda_0^o = 0$). The Z_n^o are odd about $\hat{z} = \hat{h}/2$, whilst the Z_n^e are even. Note that $Z_n^o = Z_n^e = \partial Z_n^o/\partial\hat{z} = \partial Z_n^e/\partial\hat{z} = 0$ on $\hat{z} = 0, \hat{h}(-1)$ so that $\tilde{\Phi}^{\mathrm{flat}}$ satisfies the boundary conditions at $\hat{z} = 0, \hat{h}(-1)$. The functions Y_n^o, Y_n^e will be sought so that both the partial differential equation (63) and the remaining boundary conditions are satisfied. Observing that both $\hat{\Phi}_{0,0}$ and the left hand side of (63) are odd functions about $\hat{z} = \hat{h}/2$, then $Y_n^e(\tilde{y}) = 0$ for all n and we need to only consider the odd part of the expansion, that is,

$$\tilde{\Phi}^{\mathrm{flat}}(\tilde{y}, \hat{z}) = \sum_{n=1}^{\infty} Z_n^o(\hat{z})Y_n^o(\tilde{y}).$$

Substituting this into (63), multiplying the resulting equation by Z_m^o for each $m = 1, 2, \ldots, \infty$, and integrating over $\hat{z} \in [0, \hat{h}(-1)]$ lead to an infinite system of fourth order ODE's for the Y_n^o, specifically

$$\sum_{n=1}^{\infty}\int_0^{\hat{h}(-1)}\left(\frac{\partial^2}{\partial\tilde{y}^2} + \frac{\partial^2}{\partial\hat{z}^2}\right)^2 Z_n^o(\hat{z})Y_n^o(\tilde{y})Z_m^o(\hat{z})\, d\hat{z}$$
$$= \int_0^{\hat{h}(-1)} F(\hat{y}, \hat{z}\hat{h}(-1 + \delta\tilde{y})/\hat{h}(-1))Z_m^o(\hat{z})\, d\hat{z},$$

where

$$F(\tilde{y}, \hat{z}) = 2\mathrm{Re}_\delta\hat{R}\left(\tilde{u}\frac{\partial\tilde{u}}{\partial\hat{z}} + \bar{u}_{0,0}\frac{\partial\tilde{u}}{\partial\hat{z}} + \tilde{u}\frac{\partial\bar{u}_{0,0}}{\partial\hat{z}}\right).$$

In practice, we truncate this up to a finite number of terms $N > 0$. The resulting system of ODE's must satisfy the boundary conditions

$$\int_0^{\hat{h}(-1)} -\hat{\Phi}_{0,0}(\beta, \tilde{y}, \hat{z})Z_m^o(\hat{z})\Big|_{\tilde{y}=0}\, d\hat{z}$$
$$= \sum_{n=1}^{N}\int_0^{\hat{h}(-1)} Z_n^o(\hat{z})Y_n^o(\tilde{y})Z_m^o(\hat{z})\, d\hat{z},$$
$$\int_0^{\hat{h}(-1)} -\frac{\partial}{\partial\tilde{y}}\hat{\Phi}_{0,0}(\beta, \tilde{y}, \hat{z})Z_m^o(\hat{z})\Big|_{\tilde{y}=0}\, d\hat{z}$$
$$= \sum_{n=1}^{N}\int_0^{\hat{h}(-1)} Z_n^o(\hat{z})(Y_n^o)'(\tilde{y})Z_m^o(\hat{z})\, d\hat{z},$$

for $m = 1, \ldots, N$ at $\tilde{y} = 0$, and $Y_m^o = (Y_m^o)' = 0$ for $m = 1, \ldots, N$ at $\tilde{y} = 2/\delta$. The resulting system is quite stiff making it difficult to solve using most standard ODE solvers; however, using a variant of Godunov's orthonormalisation method[45] generally works quite well. The right-hand boundary condition can also be moved closer to $\tilde{y} = 0$ (but still sufficiently far, for example, $\tilde{y} = \min\{4, 2/\delta\}$) in order to improve the conditioning and overall performance of the ODE solver without a significant loss in accuracy. The magnitude of the resulting Y_n^o decreases rapidly with respect to n and thus it is generally enough to compute a small number of terms. We found that 7 terms were sufficient to satisfy the boundary conditions to at least three decimal places. From the resulting $\tilde{\Phi}$, we obtain $\tilde{v}, \tilde{w}$, specifically

$$\tilde{v}(\tilde{y}, \hat{z}) \approx \sum_{n=1}^{N}\frac{-\hat{h}(-1)}{\hat{h}(-1 + \delta\tilde{y})}(Z_n^o)'\left(\frac{\hat{z}\hat{h}(-1)}{\hat{h}(-1 + \delta\tilde{y})}\right)Y_n^o(\tilde{y}),$$

$$\tilde{w}(\tilde{y}, \hat{z}) \approx \frac{\delta\hat{z}\hat{h}'(-1 + \delta\tilde{y})}{\hat{h}(-1 + \delta\tilde{y})}\tilde{v} + \sum_{n=1}^{N} Z_n^o\left(\frac{\hat{z}\hat{h}(-1)}{\hat{h}(-1 + \delta\tilde{y})}\right)(Y_n^o)'(\tilde{y}).$$

We point out that the inhomogeneous part of (63) could be ignored so that one can obtain an analytical series solution for $\tilde{\Phi}^{\mathrm{flat}}$ (which can be constructed via alternate Papkovich–Fadle eigenfunctions[46,47]), but we found the contribution of the inertia term is not insignificant and thus chose to include it.

VI. RESULTS

For convenience, we introduce

$$\bar{u}_\sim := \bar{u}_{0,0} + \epsilon\bar{u}_{1,0} + \delta^2\bar{u}_{0,1}, \quad (66)$$

and similar for $\hat{v}_\sim, \hat{w}_\sim$ which will be used throughout the discussion of results of the interior/central solution. Additionally, recalling that $\hat{u} = \hat{S}\bar{u}$, we set $\hat{u}_\sim = \hat{S}\bar{u}_\sim$. Furthermore,

we sometimes refer to the dimensionless velocity vectors $\bar{\mathbf{u}}_\sim = (\bar{u}_\sim, \hat{v}_\sim, \hat{w}_\sim)$ and $\hat{\mathbf{u}}_\sim = (\hat{u}_\sim, \hat{v}_\sim, \hat{w}_\sim)$. We first consider the properties of the solutions $\hat{\mathbf{u}}_\sim$ away from the side walls in cases where δ is small and the contribution of the boundary correction can be neglected. In Sec. VI D, the effect of the boundary corrections on the flow near the side walls is examined.

A. Rectangular duct

Consider a duct having a rectangular cross section, that is, $\hat{h}(\hat{y}) = 1$. In this case, since $\hat{h}'(\hat{y}) = 0$, the leading $\hat{w}$ component is zero, that is, $\hat{w}_{0,0} = 0$. Additionally, one finds $b = c = 0$ and the first-order corrections reduce to

$$\bar{u}_{1,0} = -\frac{2\hat{y}}{\hat{R}_0}\bar{u}_{0,0}, \qquad \hat{v}_{1,0} = -\frac{3\hat{y}}{\hat{R}_0}\hat{v}_{0,0},$$
$$\hat{w}_{1,0} = \frac{8\mathrm{Re}_\delta}{105\hat{R}_0^2}\hat{z}^2(\hat{h}-\hat{z})^2(\hat{h}-2\hat{z})(\hat{z}^2-\hat{z}\hat{h}-\hat{h}^2),$$
$$\bar{u}_{0,1} = \hat{v}_{0,1} = \hat{w}_{0,1} = 0.$$

Note that there is a clear dependence of the solutions on β coming from a common $\hat{R}_0^{-1}$ factor in $\bar{u}_{0,0}, \hat{v}_{0,0}$ and a $\hat{R}_0^{-2}$ factor coming from $\bar{u}_{1,0}, \hat{v}_{1,0}, \hat{w}_{1,0}$. Thus for $\hat{\alpha} > 0$ and increasing β, the magnitude of $\bar{\mathbf{u}}_\sim$ increases but with contributions from the first-order correction increasing faster. Since $\hat{w}_\sim$ consists only of a first-order correction, it increases faster (relative to its magnitude) than $\bar{u}_\sim, \hat{v}_\sim$. Analogous observations are made with decreasing β. Similarly the only dependence of $\hat{\alpha}$ comes from the $\hat{R}_0$ terms. Therefore, for any $\hat{\alpha} > 0$ or $\hat{\alpha} < 0$, all results will be identical given the same value of $\hat{R}_0$. The only difference made by a negative $\hat{\alpha}$ is that the magnitude of the solutions will decrease (rather than increase) as β increases and vice versa. The dimensionless solutions then depend on ϵ in one of the two ways, the first is simply to scale the magnitude of the order ϵ corrections and the second is to modify the rate at which the solutions change with respect to β through the $\hat{R}_0$ factors. On the other hand, since the order δ^2 corrections are zero, the dimensionless solutions are effectively independent of δ apart from an indirect influence of δ through Re_δ, to which both $\hat{v}_\sim$ and $\hat{w}_\sim$ are linearly proportional. Of course, the physical solutions will additionally scale with ϵ and δ according to the scalings employed in (8).

Figure 2 shows representative solutions for the modified velocity component $\bar{u}_\sim$ and the dimensionless velocity components $\hat{u}_\sim, \hat{v}_\sim, \hat{w}_\sim$ with respect to depth $\hat{z}$ at $\beta = 0$ for several different $\hat{y}$ evenly spaced over the cross section. Note that we avoid plotting $\hat{y}$ near ± 1 since our solutions do not satisfy the boundary conditions here and are thus unphysical. In (a), we see that the magnitude of $\bar{u}_\sim$ decreases with increasing $\hat{y}$. It is worth pointing out that this is the opposite to what is normally observed for square or circular ducts where the inertia of the fluid around a bend generally leads to faster flow toward the outside edge/wall. The reason for this is that the flow at small Re_δ through a rectangular channel having a small aspect ratio will favour a shorter path through the spiral (which is towards the inside edge). Furthermore, this observation is consistent with the Stokes solution for the flow in curved rectangular ducts having height smaller than the width (see, for example, Ref. 48). In (b), we see a smaller change in $\hat{u}_\sim$ with respect to $\hat{y}$, but, otherwise, $\hat{u}_\sim$ behaves similarly to $\bar{u}_\sim$. A cross flow structure is evident in (c) where $\hat{v}_\sim$ is positive (flowing towards the outside wall) for $\hat{z}$ close to 1/2 and is negative (flowing towards the inside wall) for $\hat{z}$ close to 0, 1. Similar to $\bar{u}_\sim$, the magnitude of $\hat{v}_\sim$ decreases with increasing $\hat{y}$. The change with respect to $\hat{y}$ in (a) and (c) is due to the contribution from the order ϵ correction. In (d), we see the small contribution to $\hat{w}_\sim$ coming from $\hat{w}_{1,0}$. Note that it is independent of $\hat{y}$ and significantly smaller than $\hat{v}_\sim$, almost two orders of magnitude smaller with the given parameters.

B. Trapezoidal duct

Now, consider a duct having a trapezoidal cross section characterised by the top wall having a constant slope, i.e., $\hat{h}(\hat{y}) = 1 + m\hat{y}$ (and thus $\hat{h}' = m$). To ensure $\hat{y} \in [-1, 1]$ is a valid domain we require $|m| \leq 1$ (which is achievable

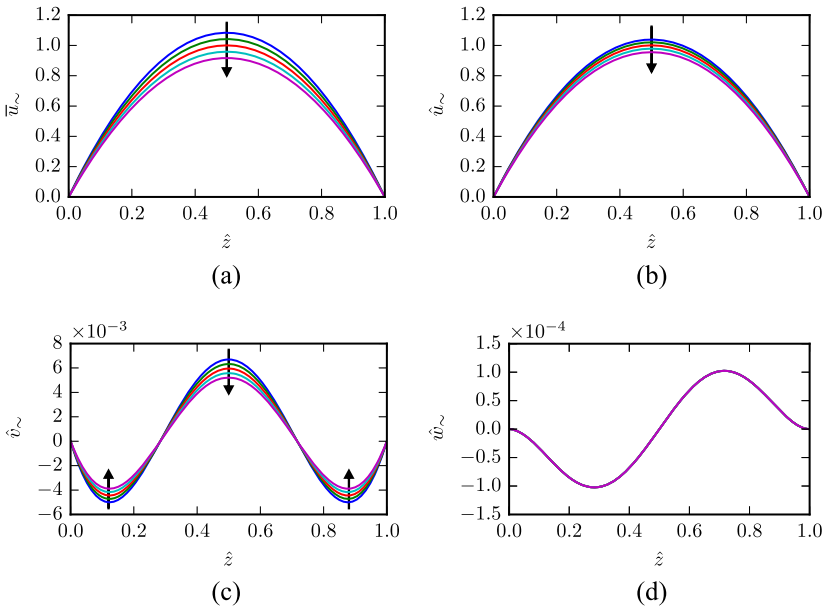

FIG. 2. Velocity components (a) $\bar{u}_\sim$, (b) $\hat{u}_\sim$, (c) $\hat{v}_\sim$, and (d) $\hat{w}_\sim$ for a rectangular duct $\hat{h}(\hat{y}) = 1$ [and thus $\hat{h}'(\hat{y}) = 0$] at $\hat{y} = -2/3$ (blue), $-1/3$ (green), 0 (red), 1/3 (cyan), 2/3 (magenta). The arrow indicates the ordering of curves corresponding to increasing $\hat{y}$ [noting in (d) all curves are identical]. Remaining parameters are $\beta = 0$, $\mathrm{Re}_\delta = 1$, $\hat{\alpha} = 2/5$, $\delta = 1/4$, and $\epsilon = 1/16$.

for more steeply sloped walls via a rescaling of parameters). In this case, the solutions are a little more complicated than for rectangular ducts since $\hat{h}' = m$ and $\hat{h}'' = \hat{h}''' = 0$, and, while the constant b (47) remains zero, the constant c (53) is non-zero (specifically $c = [52\mathrm{Re}_\delta^2((1+m)^{11} - (1-m)^{11})/24\,255 - 16m(m^2+5)]/5(m^2+1)$). As in the rectangular duct case, the dependence of the solutions on β and $\hat{\alpha}$ comes solely from the $\hat{R}_0^{-1}$ and $\hat{R}_0^{-2}$ factors. In particular, the leading order and $O(\delta^2)$ corrections of $\bar{\mathbf{u}}_\sim$ scale as $\hat{R}_0^{-1}$, whilst the $O(\epsilon)$ corrections scale as $\hat{R}_0^{-2}$.

For fixed $\hat{y}$, $\hat{h}$, the dependence of solutions on m coming from $\hat{h}'$ terms is cubic at worse. Devices of practical interest would generally be expected to satisfy $|m| \ll 1$ (for example, $m = 5/21$ in the device used by Warkiani *et al.*[15]) in which case any $(\hat{h}')^2$ and $(\hat{h}')^3$ terms could potentially be neglected such that the solutions appear to be approximately linear with respect to $\hat{h}'$. However, at the same time, m can have a big impact on the solution due to changing $\hat{h}$ as $\hat{y}$ varies. Looking at the leading order components in the form (38), $\bar{u}_{0,0}$ scales as $(1+m\hat{y})^2$, whilst $\hat{v}_{0,0}, \hat{w}_{0,0}$ scale as $(1+m\hat{y})^6$. For example, if $m = 1/5$, then the solution for $\bar{u}_{0,0}$ with fixed $\hat{z}/\hat{h}$ is approximately 1.71 times greater at $\hat{y} = 2/3$ than at $\hat{y} = -2/3$, and similarly, for $\hat{v}_{0,0}, \hat{w}_{0,0}$, the relative magnitude at $\hat{y} \pm 2/3$ is approximately a factor of 5.0 which is significant. The first-order corrections can be similarly factored to reveal analogous scalings with respect to $\hat{h}$. Additionally, the first-order corrections include terms explicitly depending on $\hat{y}$ although the effect of these is similar to that seen in the rectangular case.

The dependence on Re_δ is also more complex here. The leading order and $O(\delta^2)$ correction in $\bar{u}_\sim$ are independent of Re_δ, whilst the $O(\epsilon)$ correction is proportional to Re_δ^2. All $\hat{v}_\sim, \hat{w}_\sim$ components are proportional to Re_δ at a minimum with some of the higher order terms having contributions proportional to Re_δ^3. Mostly these are indicative of the cross-flow strength being dependent on the Reynolds number. The terms involving Re_δ^2 and Re_δ^3 tend to add a small amount of skew to $\hat{v}_\sim$ and $\hat{w}_\sim$ which is barely noticeable for $\mathrm{Re}_\delta = O(1)$. We refrain from commenting on the effect when Re_δ is large since the validity of the solutions becomes questionable because of the choice of scalings under which the solutions were obtained. Dependence of the dimensionless solutions on ϵ is similar to that in the rectangular case, that is, via the rate at which the β has an effect through the $\hat{R}_0$ terms and via the relative magnitude of the order ϵ corrections. Similarly, dependence on δ is mainly through the relative magnitude of the order δ^2 corrections as well as indirectly through Re_δ.

In Fig. 3, we plot $\bar{u}_\sim, \hat{v}_\sim, \hat{w}_\sim$ (top to bottom) for $m \in \{1/5, -1/5\}$ (left, right) for several different $\hat{y}$. Several of the trends with respect to m and $\hat{y}$ described above can be observed. For (a), (c), and (e), the magnitude of each component increases with increasing $\hat{y}$. On the other hand, in (b), (d), and (f), the opposite trend is observed with the magnitude decreasing with increasing $\hat{y}$ owing to the negative slope. Note that although m differs only in sign between (a), (c), and (e) and (b), (d), and (f), the change in magnitude with respect to $\hat{y}$ is more pronounced. This is again related to the flow tendency to favour the

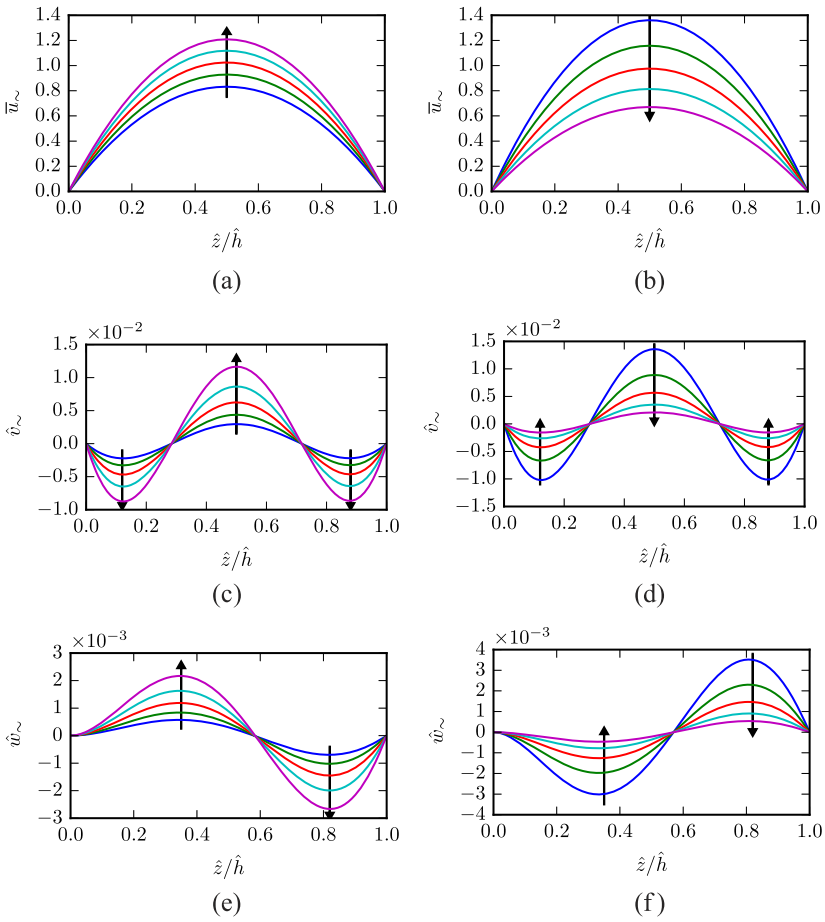

FIG. 3. Velocity $\bar{\mathbf{u}}_\sim$ for different trapezoidal ducts. (a), (c), and (e) show $\bar{u}_\sim, \hat{v}_\sim, \hat{w}_\sim$, respectively, for $\hat{h}(\hat{y}) = 1 + \hat{y}/5$, and similarly, (b), (d), and (f) are for $\hat{h}(\hat{y}) = 1 - \hat{y}/5$. In each case, the curves correspond to $\hat{y} = -2/3$ (blue), $-1/3$ (green), 0 (red), 1/3 (cyan), and 2/3 (magenta) with the arrow indicating the ordering of curves with respect to increasing $\hat{y}$. Remaining parameters are as given in Fig. 2.

shortest path toward the inside edge due to the small aspect ratio. A negative slope m effectively re-enforces this, whereas a positive slope opposes this. The sign of $\hat{w}_\sim$ also changes between (e) and (f) which is to be expected as the vertical velocity is strongly influenced by the slope. Notice that in plots (a) and (b) $\bar{u}_\sim$ differs mostly in magnitude; that is, the general shape/profile is similar for the two different slopes and for the different $\hat{y}$. A similar observation can be made for $\hat{v}_\sim$ in (c) and (d) and $\hat{w}_\sim$ in (e) and (f) up to a change in sign since $\hat{w}_\sim \propto \hat{h}'$. This is indicative of the negligible impact of contributions in the first-order corrections having a different shape/profile than the leading order solution. Whilst not evident in these plots, small to moderate changes in the ϵ, δ, Re_δ parameters do not have a noticeable impact on the general shape of the velocity profiles which suggests that the general behaviour is reasonably robust. It is also interesting to compare Figs. 3 and 2 to discern how a non-zero slope changes the solution. Comparing Figs. 2(a), 2(c) and 3(b), 3(d), observe that the general behaviour is similar but with changes in $\hat{y}$ having a greater effect on the magnitude in the latter. On the other hand, whilst Figs. 2(d) and 3(f) again have the same general shape, the latter is more skewed and has much larger magnitude. A similar comparison can be made between Figs. 2(a), 2(c), 2(d) and 3(a), 3(c), 3(e) with the exception that in the latter the magnitude of the velocity now increases with increasing $\hat{y}$ and the sign of $\hat{w}_\sim$ has changed.

C. Duct with sinusoidal top wall

Rather than continuing to consider quadratic and cubic $\hat{h}(\hat{y})$ to determine the effect of non-zero $\hat{h}''$ and $\hat{h}'''$ on the solutions, we now consider the case $\hat{h}(\hat{y}) = 1 + \sin(2\pi\hat{y})/20$ to hint at some of the other variations in solutions that are possible. Figure 4 shows the variation in the solutions $\bar{u}_\sim$, $\hat{v}_\sim$, and $\hat{w}_\sim$ at different $\hat{y}$. The $\bar{u}_\sim$ and $\hat{v}_\sim$ components have a similar profile to that seen in the rectangular and trapezoidal ducts, although the variation with respect to $\hat{y}$ is notably different. On the other hand, the behaviour of $\hat{w}_\sim$ varies qualitatively with $\hat{y}$. Variations in the magnitude, sign, and general shape/skewness of each curve can be observed owing to the dependence of $\hat{w}_\sim$ on each of $\hat{h}$, $\hat{h}'$, $\hat{h}''$, and $\hat{h}'''$. It is important to point out that for the assumption of a small aspect ratio to be valid the duct height cannot vary too much across the channel, in particular, $\hat{h}'$, $\hat{h}''$, and $\hat{h}'''$ should not be too large. For example, one cannot increase the period of the sine function used in this example by very much before seeing some erroneous behaviour due to the invalidity of the assumptions around each of the local peaks.

D. Leading order solutions with boundary corrections

So far we have looked at the leading order solution and first-order corrections in the central/interior region of the duct cross section. Here the leading order solutions with the boundary corrections are examined across the entire cross section.

Figure 5 shows contours of the leading order axial flow solutions including the correction terms near the boundaries, that is, $\bar{u}_{0,0} + \tilde{u}$ (where here $\tilde{u}$ is to be understood to include both the left and right boundary corrections). The first three plots correspond to (a) a rectangular duct with $\hat{h}(\hat{y}) = 1$, (b) a trapezoidal duct with $\hat{h}(\hat{y}) = 1 + \hat{y}/5$, and (c) a sinusoidal duct having $\hat{h}(\hat{y}) = 1 + \sin(2\pi\hat{y})/20$. In each case, we see the general behaviour in the central region which is consistent with that described above. The velocity then decays to zero in a neighbourhood of the side walls as expected. Note that the effect of the boundaries is negligible once $\hat{y}$ is approximately $\delta = 1/4$ away from the side walls. In (c), it is notable that the flow has two local maxima located where the height is maximised. Plot (d) is identical to plot (a) but with first-order correction terms included in the central solution. This illustrates that the contribution of the first-order corrections is not insignificant in the central region and is necessary to capture the feature in which the maximal axial velocity is closer to the inside wall for a rectangular duct. Although not shown here, the first-order corrections have a similar effect on the other two ducts but are

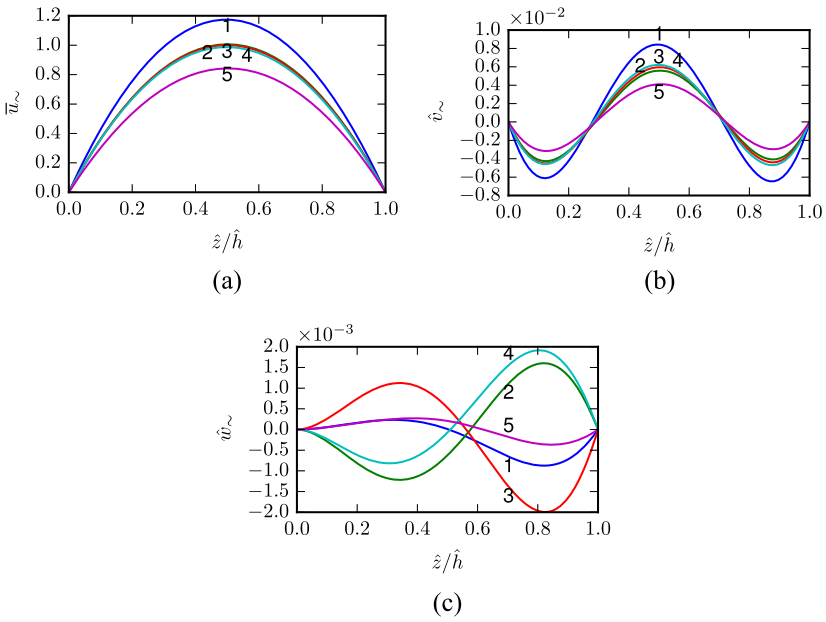

FIG. 4. Velocity components (a) $\bar{u}_\sim$, (b) $\hat{v}_\sim$, and (c) $\hat{w}_\sim$ for a duct $\hat{h}(\hat{y}) = 1 + \sin(2\pi\hat{y})/20$ at $\hat{y} = (2i - 6)/5$, $i = 1, 2, \ldots, 5$. The values of i are marked on the corresponding curves. Curves 2–4 in (a) and (b) are difficult to distinguish despite being quite different in (c). All other parameters are as given in Fig. 2.

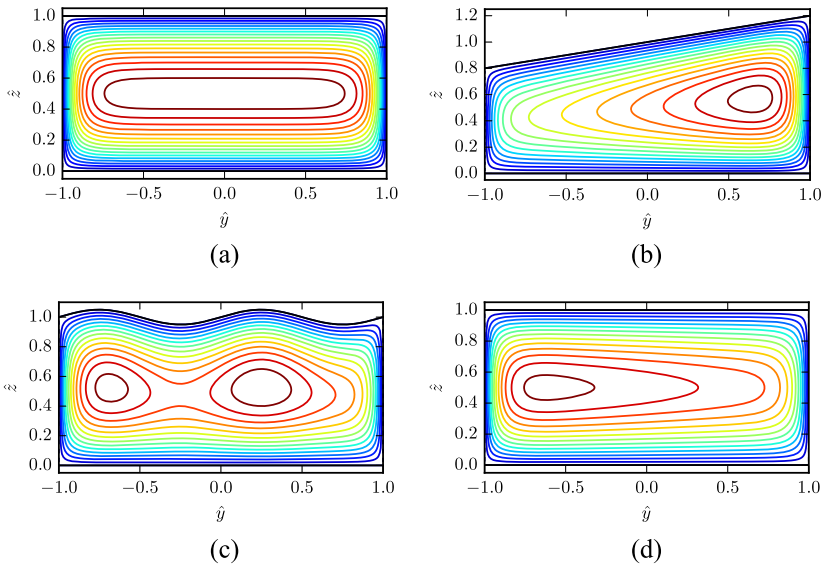

FIG. 5. Contours for the leading order axial flow $\bar{u}_{0,0}$ including the corrections near the $\hat{y} = \pm 1$ boundaries for the different duct geometries defined by (a) $\hat{h}(\hat{y}) = 1$, (b) $\hat{h}(\hat{y}) = 1 + \hat{y}/5$, and (c) $\hat{h}(\hat{y}) = 1 + \sin(2\pi\hat{y})/20$. The plot (d) is the same as (a) but with the first-order corrections added (prior to correcting near the boundaries) to illustrate their general effect. Other parameters are consistent with those used in Fig. 2.

less obvious because the effect of non-constant height is more significant.

In Fig. 6, we plot the contours of $\hat{\Phi}_{0,0} + \tilde{\Phi}$ (where here $\tilde{\Phi}$ is to be understood to include both the left and right boundary corrections) in order to visualise the streamlines of the leading order $\hat{v}_{0,0}, \hat{w}_{0,0}$ solutions with the boundary corrections included. The first three plots correspond to (a) a rectangular duct with $\hat{h}(\hat{y}) = 1$, (b) a trapezoidal duct with $\hat{h}(\hat{y}) = 1 + \hat{y}/5$, and (c) a sinusoidal duct having $\hat{h}(\hat{y}) = 1 + \sin(2\pi\hat{y})/20$. In (a), we see that the behaviour is roughly constant throughout the central region with respect to the $\hat{y}$ coordinate as expected, but near $\hat{y} = \pm 1$ we see the flow having to turn around as it approaches the walls. This is consistent with the well known behaviour of flow in curved ducts and pipes and illustrates that our simplified models for the central flow and boundary corrections perform quite well in a qualitative sense. In (b), it is easy to see the trends as $\hat{y}$ varies throughout the central region which have been discussed, and again, we see that the boundary corrections give a sensible turning around of the flow as it approaches the side walls. Note that generally the centre of the vortex pair occurs near the radial position where the axial flow is maximised. In Fig. 5(c), two local maxima of the axial flow were observed which in turn causes the secondary flow to break up into two smaller vortex pairs seen in Fig. 6(c). These two smaller vortex pairs are responsible for the significant variations in $\hat{w}_{\sim}$ with respect to the radial coordinate as observed in Fig. 4(c). Figure 6(d) is identical to (a) with the exception that first-order correction terms were added to the flow away from the side walls before constructing the boundary corrections. This demonstrates that the first-order corrections have the effect of shifting the centre of the vortices toward the inside wall.

VII. COMPARISON WITH CLASSICAL DEAN FLOW

To validate the solutions obtained via the assumption of an asymptotically small aspect ratio and curvature ratio, we compare with numerical solutions of a classical Dean flow, that is, the flow through a bent pipe or duct having constant

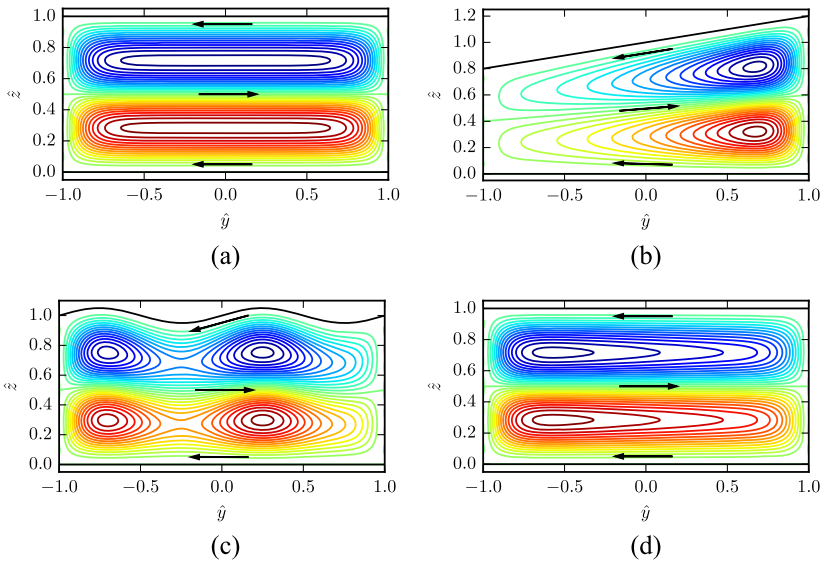

FIG. 6. Streamlines for the leading order flow $\hat{v}_{0,0}, \delta\hat{w}_{0,0}$ including the corrections near the $\hat{y} = \pm 1$ boundaries (with $N = 5$ terms), that is, $\tilde{\Phi} + \hat{\Phi}_{0,0}$, for the different duct geometries defined by (a) $\hat{h}(\hat{y}) = 1$, (b) $\hat{h}(\hat{y}) = 1 + \hat{y}/5$, and (c) $\hat{h}(\hat{y}) = 1 + \sin(2\pi\hat{y})/20$. Plot (d) is the same case as (a) except that the boundary corrections were applied to $\hat{\Phi}_{\sim} := -\int \hat{v}_{\sim}\, d\hat{z}$ as opposed to $\hat{\Phi}_{0,0}$. Arrows indicate the direction of flow. Other parameters are consistent with those used in Fig. 2.

curvature.[25] Through this comparison, it is demonstrated that the slowly changing curvature has a negligible qualitative impact on the flow. Equations equivalent to (1)–(4) of the work of Dean and Hurst[25] may be obtained from (6) by setting $\alpha = 0$ (and thus $S = R$) and, additionally, assuming that the flow is independent of β (that is, β derivatives of velocity components vanish). Following the approach of Dean and Hurst,[25] we then set $\epsilon = a/A$ and non-dimensionalise as $(y, \beta, z) = (\epsilon A\check{y}, \beta, \epsilon A\check{z})$, $\alpha = \epsilon A\check{\alpha}$, $R = A\check{R}$ (i.e., $\check{R} = 1 - \epsilon\alpha\beta + \epsilon y$), $h(y) = \epsilon A\check{h}(\check{y})$, $(Ru, v, w) = (U\check{R}\bar{\check{u}}, \sqrt{\epsilon}U\check{v}, \sqrt{\epsilon}U\check{w})$, and $p = \mu U\check{p}/\epsilon^2 A$. We also define the Dean number $\mathrm{Dn} = \sqrt{\epsilon}\mathrm{Re}$ (where $\mathrm{Re} = \rho U\epsilon A/\mu$) which is assumed to be $\mathcal{O}(1)$. Upon taking the leading order ϵ terms, the continuity equation reduces to

$$\frac{\partial\check{v}}{\partial\check{y}} + \frac{\partial\check{w}}{\partial\check{z}} = 0 \tag{67}$$

and we therefore introduce the streamfunction $\check{\Phi}$ such that $\partial\check{\Phi}/\partial\check{z} = -\check{v}$ and $\partial\check{\Phi}/\partial\check{y} = \check{w}$. The leading order terms (with respect to ϵ) in the momentum equations can then be reduced to the coupled system

$$\mathrm{Dn}\left(-\frac{\partial\check{\Phi}}{\partial\check{z}}\frac{\partial\bar{\check{u}}}{\partial\check{y}} + \frac{\partial\check{\Phi}}{\partial\check{y}}\frac{\partial\bar{\check{u}}}{\partial\check{z}}\right) = -\frac{1}{\check{R}^2}\frac{\partial\check{p}}{\partial\beta} + \left(\frac{\partial^2}{\partial\check{y}^2} + \frac{\partial^2}{\partial\check{z}^2}\right)\bar{\check{u}}, \tag{68a}$$

$$\mathrm{Dn}\left[2\check{R}\bar{\check{u}}\frac{\partial\bar{\check{u}}}{\partial\check{z}} + \left(\frac{\partial\check{\Phi}}{\partial\check{y}}\frac{\partial}{\partial\check{z}} - \frac{\partial\check{\Phi}}{\partial\check{z}}\frac{\partial}{\partial\check{y}}\right)\left(\frac{\partial^2}{\partial\check{y}^2} + \frac{\partial^2}{\partial\check{z}^2}\right)\check{\Phi}\right] = \left(\frac{\partial^2}{\partial\check{y}^2} + \frac{\partial^2}{\partial\check{z}^2}\right)^2\check{\Phi}. \tag{68b}$$

Once again we must make an assumption about the pressure which drives the flow. As the curvature is constant, it can be determined that $\partial\check{p}/\partial\beta$ is constant and so we set $\partial\check{p}/\partial\beta = -\check{G}\check{A}$ (where $\check{A} = 1$ and $\check{G}$ is a dimensionless constant for the drop in pressure per unit distance along the centre-line). Equations (68), along with no slip boundary conditions, can now be solved numerically and then compared with the solutions derived in Secs. III and IV (using a consistent choice of parameters). With the given scaling of pressure, it is straightforward to see that $\Delta P = \mu U\check{G}/\epsilon^2 A^2$. We then choose a characteristic velocity $U = \Delta P H^2/8\mu$ [recalling $H = h(0)$] in order to be consistent with the characteristic velocity used to obtain the leading order solutions in Sec. III so that a direct comparison of dimensionless velocity can be made. It then follows that $\check{G} = 8a^2/H^2$ and $\mathrm{Dn} = \sqrt{\epsilon}\rho a H^2\Delta P/8\mu^2$. For the results that follow, the finite element method with third degree Lagrangian elements has been used. Picard iterations are employed to handle the non-linear terms combined with the standard weak formulation of the resulting Poisson problem for $\bar{\check{u}}$ and a discontinuous Galerkin implementation of the biharmonic problem for $\check{\Phi}$ based upon the work of Georgoulis and Houston.[49] We discretise the two-dimensional cross section into a union of approximately 50 000 triangular cells with a 3rd degree Lagrange basis and iterations are performed until the relative error is below 10^{-12}. Further refinements were found to have a negligible impact on the solution.

There are some significant differences between Eqs. (15a) and (68) worth commenting on. The former equations were obtained by assuming asymptotically small aspect and curvature ratios and choosing the non-dimensional scalings to ensure that a cross-flow exists at leading order, which led to all but one inertial term being neglected at the leading order as well as a number of viscous and pressure terms. On the other hand, the latter equations assumed only an asymptotically small curvature ratio and were scaled to balance the majority of the viscous and inertial contributions. In addition, numerical solutions to Eqs. (68) can be obtained to satisfy the no slip boundary condition at vertical side walls (which is indeed a requirement for the problem to be well-posed), whereas our leading order solution and first-order corrections are unable to satisfy this. Furthermore, the solutions to Eqs. (15) are effectively independent for each vertical column (i.e., fixed y, β), whereas this is not the case for Eqs. (68) which would lead one to expect the latter to better resolve the flow if the fluid inertia is significant enough that variations in the top wall have a less localised impact on the flow. Despite these distinctions, we find that the solutions obtained for the two different sets of equations are close for a wide range of parameter choices. Observe that compared to our previous choice of scalings, we have $\check{y} = \hat{y}$, $\check{\alpha} = \hat{\alpha}$, $\check{z} = \delta\hat{z}$, $\check{h} = \delta\hat{h}$, $\check{R} = \hat{R}$, and $(\bar{\check{u}}, \check{v}, \check{w}) = (\bar{u}\hat{S}/\hat{R}, \sqrt{\epsilon}\hat{v}, \sqrt{\epsilon}\delta\hat{w})$. Notice that since $\hat{S}/\check{R} = 1 + O(\epsilon^2)$ and our approximation of $\bar{u}$ is only up to order ϵ, it suffices to compare $\bar{\check{u}}$ and $\bar{u}$ directly. When comparing the v, w components of numerical solutions of Eqs. (68) with the solutions $\bar{\mathbf{u}}_\sim$, we scale the former to match the latter: that is, the rescaled Dean flow solutions $(\bar{u}_d, \hat{v}_d, \hat{w}_d) := (\bar{\check{u}}, \check{v}/\sqrt{\epsilon}, \check{w}/\sqrt{\epsilon}\delta)$ can be compared directly with $(\bar{u}_\sim, \hat{v}_\sim, \hat{w}_\sim)$. All comparisons will be made at $\beta = 0$ as the results are similar at $\beta \neq 0$ (provided one sets the A used to solve the Dean equations equal to the spiral radius $A - \alpha\beta$ at the given β).

Figure 7 compares the components of $\mathbf{u}_d = (\bar{u}_d, \hat{v}_d, \hat{w}_d)$ and $\bar{\mathbf{u}}_\sim$ for the two cases $\hat{h}(\hat{y}) = 1$ (left column) and $\hat{h}(\hat{y}) = 1 + \hat{y}/5$ (right column) at $\beta = 0$ along the lines $\hat{y} = -1/2, 0, 1/2$. There is no observable difference in the axial and radial components of the velocity in both cases. Some deviation in the magnitude of the vertical velocity can be observed but, as the magnitude of this component is negligible compared to the others, this difference is not highly significant. Although not shown here, results for the case of the sinusoidal height function $\hat{h}(\hat{y}) = 1 + \sin(2\pi\hat{y})/20$ are qualitatively similar. The comparison when plotting for the other values of $\hat{y}$ sufficiently far from $\hat{y} = \pm 1$ gives qualitatively similar results. In a neighbourhood of $\hat{y} = \pm 1$, the two solutions will begin to differ significantly as $\mathbf{u}_d \to 0$ (since it satisfies the no slip boundary condition).

Figure 8 shows streamlines of $\hat{v}_d, \hat{w}_d$ for qualitative comparison with the leading order streamlines of the solutions $\hat{v}_{0,0}, \hat{w}_{0,0}$ including boundary corrections as shown in Fig. 6. The qualitative agreement between Figs. 8(a)–8(c) and 6(d), 6(b), and 6(c) is quite good, noting that the first-order correction of our solutions in the rectangular case is required to capture the centre of the vortex of the Dean solution being shifted toward the inside wall. We point out that Warkiani *et al.*[15] separated circulating tumour cells (CTCs) from white blood cells (WBCs) using a trapezoidal duct similar to that depicted in Fig. 8(b) as they found this design favourable for separation because the WBCs became trapped in the Dean vortex located toward the outer wall, whereas the CTCs focused toward the inner wall. One could imagine that ducts similar

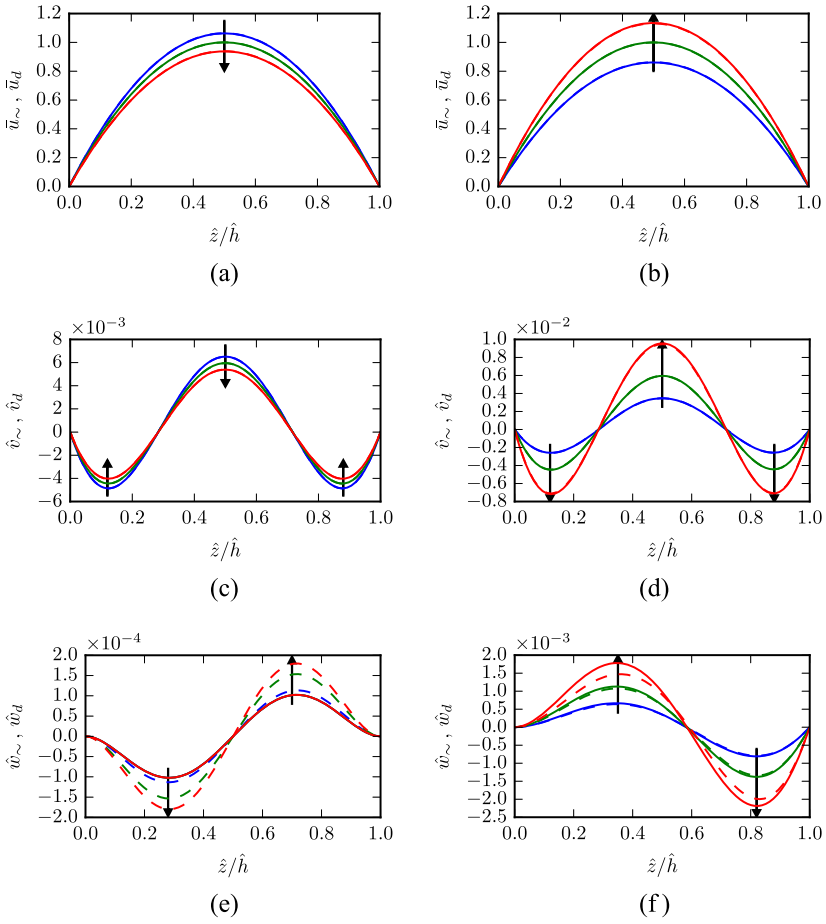

FIG. 7. Comparison of the velocities $\bar{u}_\sim$, $\bar{u}_d$ in (a) and (b), $\hat{v}_\sim$, $\hat{v}_d$ in (c) and (d), and $\hat{w}_\sim$, $\hat{w}_d$ in (e) and (f) for the flow through a rectangular duct with $\hat{h}(\hat{y}) = 1$ [(a), (c), and (e)] and through a trapezoidal duct with $\hat{h}(\hat{y}) = 1 + \hat{y}/5$ [(b), (d), and (f)]. Here $(\bar{u}_d, \hat{v}_d, \hat{w}_d)$ (dashed) are numerical solutions for the Dean flow rescaled to match the scaling used to obtain $(\bar{u}_\sim, \hat{v}_\sim, \hat{w}_\sim)$ (solid). Arrows indicate the ordering of curves corresponding to $\hat{y} = -1/2$, 0, 1/2 which are also coloured blue, green, and red, respectively. Remaining parameters are chosen to be consistent with Fig. 2.

to that depicted in Fig. 8(c) may also potentially separate different particles/cells by trapping them in the two distinct pairs of vortices that occur across the duct cross section. Contour plots for the axial flow are omitted as they appear identical to Figs. 5(d), 5(b), and 5(c).

We next investigate the convergence of our solutions to numerical solutions of the Dean flow as ϵ decreases. Let Ω denote the cross section at $\beta = 0$, specifically

$$\Omega = \{(\hat{y}, \hat{z}) : \hat{y} \in [-1, 1], \hat{z} \in [0, \hat{h}(\hat{y})]\}. \tag{69}$$

The relative difference between numerical Dean flow solutions $(\bar{u}_d, \hat{v}_d, \hat{w}_d)$ and our solutions (both with and without the boundary and first-order corrections) is considered. Defining

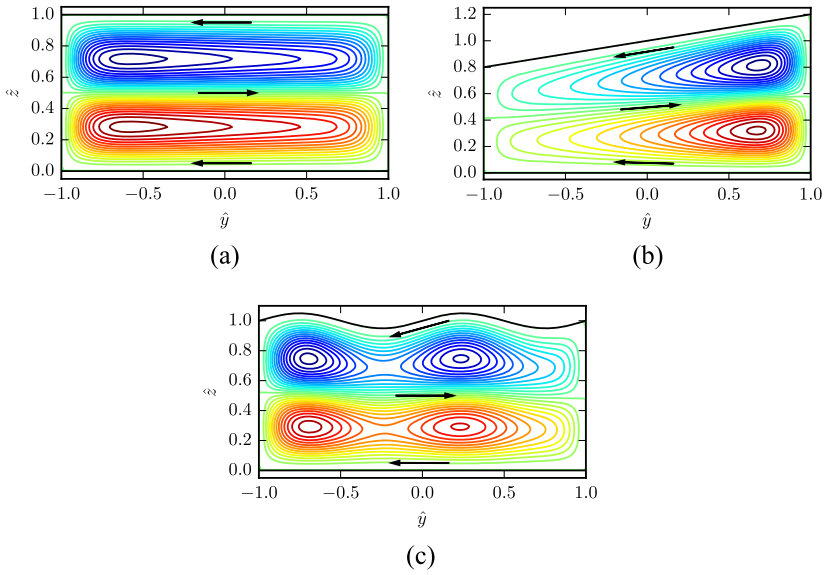

FIG. 8. Streamlines computed from numerical solutions of (68) for the duct geometries (a) $\hat{h}(\hat{y}) = 1$, (b) $\hat{h}(\hat{y}) = 1 + \hat{y}/5$, and (c) $\hat{h}(\hat{y}) = 1 + \sin(2\pi\hat{y})/20$. Arrows indicate the direction of flow. Other parameters are consistent with those used in (a)–(c) in Fig. 6.

$$E(\bar{u}_d, \bar{u}_{0,0}) := \frac{\|\bar{u}_d - \bar{u}_{0,0}\|_2}{\|\bar{u}_d\|_2}, \tag{70}$$

where $\|\cdot\|_2$ is the usual L_2 norm over the cross section Ω, we compute the relative difference between the Dean solution and our solution, with and without the different correction terms, for each of the three different duct shapes considered thus far over a range of different ϵ and δ. Recalling that $\bar{u}_{0,0}, \hat{v}_{0,0}, \hat{w}_{0,0}$ denote the leading order dimensionless flow components and taking $\tilde{u}, \tilde{v}, \tilde{w}$ denote the boundary corrections for these near $\hat{y} = -1$, 1 we compute $E(\bar{u}_d, \bar{u}_{0,0})$, $E(\bar{u}_d, \bar{u}_{0,0} + \tilde{u})$ and similar for the v, w components. Additionally, with $\bar{u}_\sim, \hat{v}_\sim, \hat{w}_\sim$ denoting the leading order solution plus first-order corrections as in (66) and $\tilde{u}_\sim, \tilde{v}_\sim, \tilde{w}_\sim$ denoting the boundary corrections associated with these, we also compute $E(\bar{u}_d, \bar{u}_\sim + \tilde{u}_\sim)$ and similar for the v, w components. Figures 9(a), 9(c), and 9(e) show the convergence of the different $E(\cdot,\cdot)$ as ϵ decreases for fixed $\delta = 1/8$, while (b), (d), and (f) show the convergence for $\delta = \sqrt{\epsilon}$. We used the first 16 non-zero modes in constructing the boundary correction $\tilde{u}$ and 7 modes in constructing the boundary corrections $\tilde{v}, \tilde{w}$, which in each case ensured that boundary conditions were satisfied to at least 3 decimal places. In (a), (c), and (e), the difference between the Dean solution and our leading order solution (blue curves) become, almost immediately, constant with respect to ϵ for all three duct geometries as the error becomes dominated by the differences near the boundaries. The error is particularly high in the $\hat{w}$ component since our leading order solutions do not capture the behaviour near the $\hat{y} = \pm 1$ boundaries where $\hat{w}$ is most significant. Upon adding the boundary corrections to our solutions (green curves), all three velocity components converge to $(\bar{u}_d, \hat{v}_d, \hat{w}_d)$ at the rate $O(\epsilon)$. For very small ϵ and non-rectangular ducts, this does eventually reach a limit whereupon the error is dominated by $O(\delta)$ terms arising from the error associated with the construction of the boundary correction. Upon adding both the first-order and boundary corrections (red curves), the relative differences become even smaller. Convergence is initially at a rate $O(\epsilon^2)$ for the $\bar{u}, \hat{v}$ velocities before reaching a limit where $O(\delta)$ errors are again most significant. The $\hat{w}$ components are also closer but to a lesser extent owing to the most significant contribution being near the $\hat{y} = \pm 1$ boundaries. In (b), (d), and (f), we see that convergence in $\bar{u}_{0,0}, \hat{v}_{0,0}$ toward $\bar{u}_d, \hat{v}_d$ (blue curves) is approximately order $\delta^{1/2}$ owing to the error being dominated in a neighbourhood of the boundaries. As before, there is essentially no convergence in the $\hat{w}$ component in the absence of the boundary correction. With the boundary correction (green curves), we see that all three components converge at the rate $O(\epsilon)$ [or equivalently $O(\delta^2)$] as is expected. When both first-order and boundary corrections are present (red curves), convergence in the $\hat{u}, \hat{v}$ components is greatly improved, initially at a rate $O(\epsilon^2)$ and then slowing to $O(\epsilon)$ for the non-rectangular ducts. The $\hat{w}$ component is also improved but to a lesser extent, again since error is dominated by the contribution near the $\hat{y} = \pm 1$ boundaries. We conclude from these results that when both ϵ and δ are small, then the leading order flow in a spiral duct at a specific

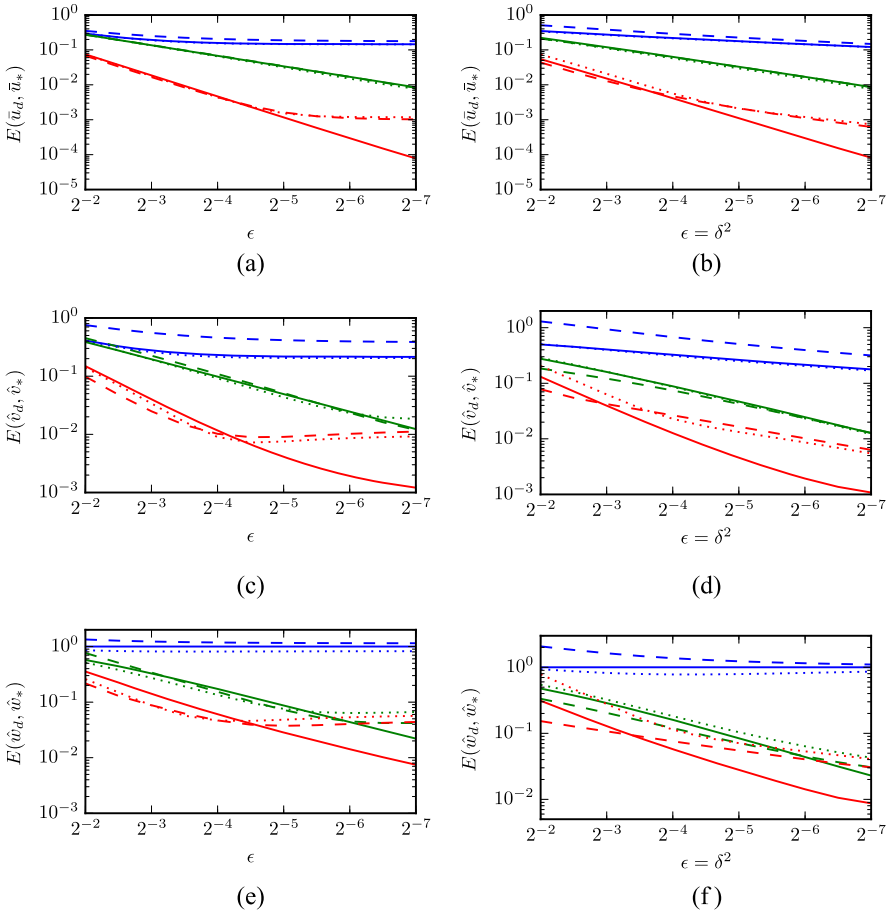

FIG. 9. Convergence of $E(\bar{u}_d, \bar{u}_*)$ for $\bar{u}_* \in \{\bar{u}_{0,0}, \bar{u}_{0,0} + \tilde{u}, \bar{u}_\sim + \tilde{u}_\sim\}$ (blue, green, and red, respectively, see the text) with respect to ϵ for the duct shapes $\hat{h}(\hat{y}) = 1$ (solid), $\hat{h}(\hat{y}) = 1 + \hat{y}/5$ (dashed), and $\hat{h}(\hat{y}) = 1 + \sin(2\pi\hat{y})/20$ (dotted). Plot (a) has fixed $\delta = 1/8$, whilst (b) has varying $\delta = \sqrt{\epsilon}$. Plots (c) and (d) show similar for $E(\hat{v}_d, \hat{v}_*)$ and (e) and (f) show similar for $E(\hat{w}_d, \hat{w}_*)$. Remaining parameters are $\mathrm{Re}_\delta = 1$, $\beta = 0$ and $\hat{\alpha} = 2/5$.

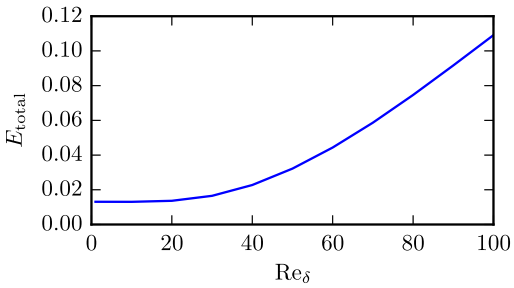

FIG. 10. E_{total} vs Re_δ for the trapezoidal duct used by Warkiani *et al.*[15]

β is not significantly different from that in a curved duct having curvature the same as that as the spiral duct at that particular β. It is evident that the boundary corrections are necessary to obtain a good description of the flow in a global sense, albeit our solution is particularly good away from the side walls for small δ. With the boundary corrections included, our solutions provide a reasonable description of the flow even for moderate δ and ϵ, particularly with both the first-order and boundary corrections. Finally, we point out that, in the case of a spiral duct, as a flow progresses the curvature parameter ϵ continuously changes and therefore the plots (a), (c), and (e) in Fig. 9 give some indication as to how the accuracy of our solutions can vary throughout a spiral of fixed geometry.

Finally, we look at how close our approximate solutions are to the Dean flow for increasing Re_δ. For this study, we approximate the flow in the middle of the spiral duct having trapezoidal cross section used by Warkiani *et al.*[15] Over a range of Re_δ, we measure the L_2 error of the dimensional velocity vector, that is,

$$E_{\text{total}} = \left\| \left(\hat{R}\bar{u}_d, \epsilon\hat{v}_d, \epsilon\delta\hat{w}_d\right) - \left(\hat{R}\bar{u}_{0,0}, \epsilon\hat{v}_{0,0}, \epsilon\delta\hat{w}_{0,0}\right) - \left(\hat{R}\tilde{u}, \epsilon\tilde{v}, \epsilon\delta\tilde{w}\right) \right\|_2 / \left\| \left(\hat{R}\bar{u}_d, \epsilon\hat{v}_d, \epsilon\delta\hat{w}_d\right) \right\|_2 . \quad (71)$$

This demonstrates how well our solution approximates the flow velocity vector in a real device (assuming that the effect of varying curvature is indeed negligible) and gives some indication of the range of Re_δ for which our solution is valid. Figure 10 shows that E_{total} is approximately constant over $\text{Re}_\delta \in [0, 20]$, begins to increase slowly over $\text{Re}_\delta \in [20, 50]$, and then increases approximately linearly over $\text{Re}_\delta \in [50, 100]$. The degradation in accuracy for large Re_δ occurs as the fluid inertia becomes more significant increasing the magnitude of the flow near the outside wall, an effect which is not captured by our leading order solutions. Results are qualitatively similar for other duct shapes. From this, we conclude that our solutions are valid for $\text{Re}_\delta = O(10)$, an order of magnitude larger than the initial assumption. In particular, this includes the range of Re_δ of [7.5, 15] that we estimate for the experiments of Warkiani *et al.*[15]

VIII. CONCLUDING REMARKS

Solutions for the flow through a spiral microfluidic duct having an asymptotically small aspect ratio and curvature have been derived. A difficulty that arises in using lubrication theory for this problem is imposing the correct boundary corrections at the side walls, but we demonstrate how simple series approximations may be obtained in the neighbourhood of the walls to rectify the flow in these regions. The results show that our solutions provide a good approximation of the Dean flow, particularly for small values of ϵ, δ. From this, we conclude that the slowly changing curvature has a negligible impact on the flow other than to modify the strength of the cross flow as β changes.

First-order corrections in the central region have also been derived and these further improve the accuracy in this region when δ is small. Additionally we find our solutions to be valid for $\text{Re}_\delta = O(10)$ which includes the range seen in some experiments. For larger values of Re_δ, ϵ, and/or δ where the error of the solutions may be larger than desired, the simplicity of these solutions may still make them useful in providing a good initial guess for direct numerical simulations. Our approximate solutions are mesh-less in the sense they describe the flow through ducts in which the shape of the top wall may change without the need to discretise the domain. When δ is small, one can easily and quickly examine the part of solution valid away from the side walls to determine if there will be local maxima and/or minima in the axial flow due to the local changes in the duct height which may lead to the break up of the vortex pair in the secondary flow. The simple and quickly computable form of the solutions obtained is expected to be useful for studying the behaviour of particles in the flow, which is the primary motivation for this work.

It is clear from the multi-nomial expansion in ϵ, δ^2 that contributions of second-order terms is bounded above by the larger of $\{\delta^4, \delta^2\epsilon, \epsilon^2\}$. Since the ducts of interest to us have small δ^2 and ϵ, we expect that such terms will not qualitatively change the flow solution (quantitatively the relative contribution is expected to be much less than 1%). Additionally, the derivation of second-order corrections, whilst continuing to allow an arbitrary top wall shape, including consistent corrections at the side walls, is significantly more cumbersome. For these reasons, we did not go on to consider second-order corrections and would suggest that an alternative approach may be better suited to situations in which higher order corrections may become important.

ACKNOWLEDGMENTS

This research was supported under Australian Research Council's Discovery Projects funding scheme (Project No. DP160102021).

[1] J. M. Martel and M. Toner, "Inertial focusing in microfluidics," Annu. Rev. Biomed. Eng. **16**, 371–396 (2014).
[2] G. Segre and A. Silberberg, "Radial particle displacements in Poiseuille flow of suspensions," Nature **189**, 209–210 (1961).
[3] H. L. Goldsmith and S. G. Mason, "Axial migration of particles in Poiseuille flow," Nature **190**, 1095–1096 (1961).
[4] F. P. Bretherton, "Slow viscous motion round a cylinder in a simple shear," J. Fluid Mech. **12**, 591–613 (1962).
[5] P. G. Saffman, "The lift on a small sphere in a slow shear flow," J. Fluid Mech. **22**, 385–400 (1965).
[6] R. G. Cox and H. Brenner, "The lateral migration of solid particles in Poiseuille flow—I theory," Chem. Eng. Sci. **23**, 147–173 (1968).
[7] B. P. Ho and L. G. Leal, "Inertial migration of rigid spheres in two-dimensional unidirectional flows," J. Fluid Mech. **65**, 365–400 (1974).

[8]P. Vasseur and R. G. Cox, "The lateral migration of a spherical particle in two-dimensional shear flows," J. Fluid Mech. **78**, 385–413 (1976).
[9]P. Ganatos, S. Weinbaum, and R. Pfeffer, "A strong interaction theory for the creeping motion of a sphere between plane parallel boundaries. Part 1. Perpendicular motion," J. Fluid Mech. **99**, 739–753 (1980).
[10]D. Leighton and A. Acrivos, "The shear-induced migration of particles in concentrated suspensions," J. Fluid Mech. **181**, 415–439 (1987).
[11]J. A. Schonberg and E. J. Hinch, "Inertial migration of a sphere in Poiseuille flow," J. Fluid Mech. **203**, 517–524 (1989).
[12]E. S. Asmolov, "The inertial lift on a spherical particle in a plane Poiseuille flow at large channel Reynolds number," J. Fluid Mech. **381**, 63–87 (1999).
[13]K. Hood, S. Lee, and M. Roper, "Inertial migration of a rigid sphere in three-dimensional Poiseuille flow," J. Fluid Mech. **765**, 452–479 (2015).
[14]D. Di Carlo, "Inertial microfluidics," Lab Chip **9**, 3038–3046 (2009).
[15]M. E. Warkiani, G. Guan, K. B. Luan, W. C. Lee, A. A. S. Bhagat, P. Kant Chaudhuri, D. S.-W. Tan, W. T. Lim, S. C. Lee, P. C. Y. Chen, C. T. Lim, and J. Han, "Slanted spiral microfluidics for the ultra-fast, label-free isolation of circulating tumor cells," Lab Chip **14**, 128–137 (2014).
[16]C. Liu, C. Xue, J. Sun, and G. Hu, "A generalized formula for inertial lift on a sphere in microchannels," Lab Chip **16**, 884–892 (2016).
[17]A. Shamloo and A. Mashhadian, "Inertial particle focusing in serpentine channels on a centrifugal platform," Phys. Fluids **30**, 012002 (2018).
[18]M. R. Maxey and J. J. Riley, "Equation of motion for a small rigid sphere in a nonuniform flow," Phys. Fluids **26**, 883–889 (1983).
[19]T. R. Auton, J. C. R. Hunt, and M. Prud'Homme, "The force exerted on a body in inviscid unsteady non-uniform rotational flow," J. Fluid Mech. **197**, 241–257 (1988).
[20]E. Loth and A. J. Dorgan, "An equation of motion for particles of finite Reynolds number and size," Environ. Fluid Mech. **9**, 187–206 (2009).
[21]J. M. Martel and M. Toner, "Inertial focusing dynamics in spiral microchannels," Phys. Fluids **24**, 032001 (2012).
[22]J. Zhou and I. Papautsky, "Fundamentals of inertial focusing in microchannels," Lab Chip **13**, 1121–1132 (2013).
[23]W. R. Dean, "Note on the motion of fluid in a curved pipe," London, Edinburgh, Dublin Philos. Mag. J. Sci. **4**, 208–223 (1927).
[24]S. A. Berger, L. Talbot, and L.-S. Yao, "Flow in curved pipes," Annu. Rev. Fluid Mech. **15**, 461–512 (1983).
[25]W. R. Dean and J. M. Hurst, "Note on the motion of fluid in a curved pipe," Mathematika **6**, 77–85 (1959).
[26]C. Y. Wang, "On the low-Reynolds-number flow in a helical pipe," J. Fluid Mech. **108**, 185–194 (1981).
[27]M. Germano, "On the effect of torsion on a helical pipe flow," J. Fluid Mech. **125**, 1–8 (1982).
[28]M. Germano, "The dean equations extended to a helical pipe flow," J. Fluid Mech. **203**, 289–305 (1989).
[29]H. C. Kao, "Torsion effect on fully developed flow in a helical pipe," J. Fluid Mech. **184**, 335–356 (1987).
[30]E. R. Tuttle, "Laminar flow in twisted pipes," J. Fluid Mech. **219**, 545–570 (1990).
[31]L. Zabielski and A. J. Mestel, "Steady flow in a helically symmetric pipe," J. Fluid Mech. **370**, 297–320 (1998).
[32]D. G. Lynch, S. L. Waters, and T. J. Pedley, "Flow in a tube with non-uniform, time-dependent curvature: Governing equations and simple examples," J. Fluid Mech. **323**, 237–265 (1996).
[33]D. Gammack and P. E. Hydon, "Flow in pipes with non-uniform curvature and torsion," J. Fluid Mech. **433**, 357–382 (2001).
[34]K. H. Winters, "A bifurcation study of laminar flow in a curved tube of rectangular cross-section," J. Fluid Mech. **180**, 343–369 (1987).
[35]D. Manoussaki and R. S. Chadwick, "Effects of geometry on fluid loading in a coiled cochlea," SIAM J. Appl. Math. **61**, 369–386 (2000).
[36]C. Pozrikidis, "Stokes flow through a coiled tube," Acta Mech. **190**, 93–114 (2007).
[37]M. Norouzi and N. Biglari, "An analytical solution for dean flow in curved ducts with rectangular cross section," Phys. Fluids **25**, 053602 (2013).
[38]Y. M. Stokes, B. R. Duffy, S. K. Wilson, and H. Tronnolone, "Thin-film flow in helically wound rectangular channels with small torsion," Phys. Fluids **25**, 083103 (2013).
[39]S. Lee, Y. M. Stokes, and A. L. Bertozzi, "Behavior of a particle-laden flow in a spiral channel," Phys. Fluids **26**, 043302 (2014).
[40]D. J. Arnold, Y. M. Stokes, and J. E. F. Green, "Thin-film flow in helically-wound rectangular channels of arbitrary torsion and curvature," J. Fluid Mech. **764**, 76–94 (2015).
[41]D. J. Arnold, Y. M. Stokes, and J. E. F. Green, "Thin-film flow in helically wound shallow channels of arbitrary cross-sectional shape," Phys. Fluids **29**, 013102 (2017).
[42]J. M. Hill and Y. M. Stokes, "A note on Navier–Stokes equations with nonorthogonal coordinates," ANZIAM J. **59**, 335–348 (2018).
[43]R. Aris, *Vectors, Tensors: And the Basic Equations of Fluid Mechanics*, Prentice-Hall International Series in the Physical and Chemical Engineering Sciences (Prentice-Hall, 1962).
[44]P. N. Shankar, "On the use of biorthogonality relations in the solution of some boundary value problems for the biharmonic equation," Curr. Sci. **85**, 975–979 (2003).
[45]S. D. Conte, "The numerical solution of linear boundary value problems," SIAM Rev. **8**, 309–321 (1966).
[46]D. D. Joseph, "The convergence of biorthogonal series for biharmonic and Stokes flow edge problems. Part I," SIAM J. Appl. Math. **33**, 337–347 (1977).
[47]D. D. Joseph and L. Sturges, "The convergence of biorthogonal series for biharmonic and Stokes flow edge problems: Part II," SIAM J. Appl. Math. **34**, 7–26 (1978).
[48]C. Wang, "Stokes flow in a curved duct—A Ritz method," Comput. Fluids **53**, 145–148 (2012).
[49]E. H. Georgoulis and P. Houston, "Discontinuous Galerkin methods for the biharmonic problem," IMA J. Numer. Anal. **29**, 573–594 (2009).